List of changes

3 Field observation.

It has been clarified, that water-bearing minerals are rare, and that pseudotachylyte do not show an affinity to „wetter" assemblages.

Figure 3

Figure caption is more descriptive

Figure 4

Backscatter images c) and d) were added to better illustrate the multiple generations.

4.1 Post-shearing pseudotachylytes

The use of the quenched mineral assemblage for geothermobarometry is discussed in more detail.

4.2 Syn-shearing pseudotachylytes

The description of sample F31 was added, to illustrate the switch from brittle to ductile and back.

The amount of water bearing minerals has been clarified.

Information of the identification of kyanite was added.

Paragenesis for S6 has been added.

Crystallization of garnet is discussed now.

4.3 Sheared pseudotachylyte in undeformed host rock

The description of sample F44 was improved with regard to the comments of the reviewers.

Figure 5

Figure d) has been integrated from the Appendix.

Figure 6

Has been added to illustrate multiple generations of pseudotachylyte with phases of ductile shearing in between.

Figures 7,8,9

Bounding red box for the observed assemblages was added to the pseudo-section plots.

Figure 9

Minerals are now labeled in c).

6 Summary

Text was modified to replace the term "cyclic".

The resulting geothermal gradient is now presented.

7 Discussion

Self-localizing thermal runaway is now discussed in more detail.

A remark about stresses propagating upwards from the strong mantle was added.

Appendix C

A table with a summary of outcrop locations mentioned in the text was added.

Andersen

RC: You have not shown that they are cyclic, to me the changes from brittle to ductile and back again seem random (not cyclic).
AR: With the word "cyclic" we wanted to express that deformation is changing from brittle to ductile and back. We try to demonstrate this by pointing out, that pseudotachylytes are emplaced pre-, syn- and post shearing.
AC: We integrated a new Fig 6 to show that sheared pseudotachylytes can be found as clasts in a new generation of pseudotachylyte, demonstrating the switch from brittle to ductile to brittle again, which may actually repeat several times. We now restrict the use of the term "cycles" to the discussion and specifically with reference to earthquake cycles.

RC: How these repeated 'strong variations' in stresses are formed, and the causal link between stress variations and the formation of shear zones vs. co-seismic faulting is not discussed or explained in detail in the manuscript.
AR: In the discussion, we test our observations against the common proposed models for brittle-ductile interplay in the lower crust. With the data presented here, we cannot establish the cause of the stress variations. This problem will be specifically addressed in a different manuscript, which is currently in preparation. The aim of the current manuscript is different and quite specific – to establish that repeated cycles from brittle to ductile to brittle, involving large volumes of pseudotachylyte, are occurring under water deficient conditions of ca. 650 °C and 1.2 GPa, i.e. lower crustal conditions

RC: Self-localised thermal runaway (SLTR) following John et al (2009) is plainly rejected as a weakening mechanism in this manuscript because the authors have not found ductile precursors to any of the studied faults. I wonder if they have looked well enough? because there is no detailed description or illustration of fault veins in their figures included here. The deep crustal PST examples I have detailed knowledge from (in Corsica and Norway) we have spent a long time looking and dedicated sampled fault veins (not the nice big injection veins) to observe what happens with wall-rocks during co-seismic faults. Particularly the smallest fault veins (see Andersen et al 2008, Deseta et al. 2014) provide the best examples of ductile wall-rock damage zones. The evidence for crystal-plastic and ductile deformation is not easily found because the high heat tends to melt and destroy the evidence for the ductile wall-rock precursor as well as most of the inclusions of the wall rocks. Therefore, only a few examples provide macroscopic evidence for pre-fault (PST) ductile fabrics, one is from the Kråkeneset gabbro described in John et al. (2009) and I enclose a field photo of this for your inspection, where shear fabrics are preserved along a small fault next to a PST where they are mostly melted away on the same fault. Evidence from minor fault in thin section are more common.Therefore, if you still find no evidence of shearing after new inspection of wall-rock damage zones in you fault veins, you are at least be able to say with confidence that evidence of SLTR is not found after careful inspection! Otherwise, perhaps you should keep an open mind to SLTR as an option until you can document that there is no crystal plasticity or ductility anywhere in the wall-rock damage zones along your fault veins. […] And I want image(s) fault-vein contacts with wall-rocks.
AR: We tried to have an unbiased view with regard to the formation mechanism of the pseudotachylytes in the Musgrave Block. The observations we made are in conflict with the idea of SLTR. In the new Fig. 6, we present a pseudotachylyte fault vein including the host rock, where no ultramylonitic precursor is visible. A more thorough discussion is presented in the short comment (SC1) in the discussion. We did not add a more thorough discussion to the current manuscript, as it is beyond the scope and aim of this study.

RC: In the PST in Holsnøy described by Austrheim and co-workers, mineral inclusions in for example garnet is very commonly associated with the shock-type deformation (partial pulverisation of wall-rocks) of minerals during the co-seismic faulting, and should therefore perhaps be included?

AR: We do report fractured garnets, but they show discrete and rather planar fractures and are not pulverized.
AC: The connection between fractured garnet and seismic stresses is now added to the text, together with relevant references.

RC: Figures! In this part of my review with general comments I suggest that you improve most of your figures or at least the explanation in the figure text. If you discuss more in text I want you to specify where this can be found in the main text. I also want to see micrograph of fault-veins and I want better (in fact much improved) text to most of the figures. In many cases texts are very short and do not explain well enough what we see particularly in the photo figures. There are also some errors for examples in Fig 8b where the pressure unit is written as GPa but probably given in numbers as kbar? […]
In Fig. 3 you have some nice PST images, but again the explanations in the fig-text is very short and inadequate. I miss a much better explanation of what I see in fig 3a and 3c, and a discussion/explanation of how rotation of clasts in 3a occurred, and if there is a PST fault vein along the contact with the amphibolite dolerite and the duplex-like structure in 3b. This can be done better!
AC: Figure captions have been improved to aid a better understanding of the images. However, in principle, we consider that figure captions should be concise and limited to description rather than interpretation. The figures are all described and discussed in detail within the main body of the text. We apologize for the error made in Fig 8b, which has been corrected.

RC: A regional geological map (Fig. 2) should normally have a regional cross-section as well.
AR: In our opinion, the geophysical maps are more instructive for the purpose than a geological map, as these also see through the cover providing a clearer tectonic interpretation and highlighting the difference between Mulga Park- and Fregon Subdomains, as well as the post-Musgrave Orogeny granites that were not depleted in Th.
AC: We included a recent reference (Wex et al. 2017) where a geological map and cross sections can be found.

RC: In figure 4 there is an inset backscatter image of an obliquely foliated injection vein? Explain what we see and why is there a foliation there. Is this flow foliation or some post PST deformation phenomenon?
AR: As the foliation is slightly oblique to the margin of the vein, we interpret the foliation to be the result of ductile shearing.
AC: This has been clarified in the text.

RC1_supplement: Other comments, if not already addressed above, have been integrated in text and figures.

RC: Silicate melts may have a high fluid, any info on the content of fluids in the pst?
AR: As clearly shown in the sample description, biotite is the only water-bearing mineral observed in the studied sample (F68). Furthermore, kyanite rather than clinozoisite/epidote is present in the pseudotachylyte, also indicating that the fluid content of the initial melt was low.

RC: injection vein with later localisation? (comment of Fig. 3b)
AR: The geometries are not clear enough, to call this an injection vein. The ductile overprint is later, as stated in the text.

RC: is there any evidence for quenched mineral zoning as evidence for progressive cooling?
AR: The grain size of minerals is extremely small, and no zoning is visible.

RC: Do we see two generations of pst or just a transition from foliated to not foliated? Text is not adequate for reader to understand this brittle- to ductile transition. Explain better! I think more illustrations are required, also optical micrograph, to me this could look as a ductile precursor to a static quenched pst! (comment to Fig.5a)

AR: The host rock is a quartzo-feldspathic mylonite, with clearly visible quartz ribbons (appear dark). We here want to demonstrate the brittle overprint of the mylonitic foliation. There is no evidence, that the mylonite represents a ductile precursor. Also, in the model of John et al. (2009), the precursor (ultra-) mylonite is expected to be completely melted.

AC: The figure captions have been improved to clarify this.

RC: Is there any issue between cooling from max shear heating (friction) temperatures and temperatures derived from mineral equilibria modelling? Could there have been superheating?

AR: As the temperatures are derived from equilibria modelling of dynamically recrystallized minerals and not on minerals directly crystallizing from a melt, we are confident that superheating effects are not reflected in the mineral compositions.

RC: P-1.2 GPa and 690C are considerably more narrow than the pseudosection shows, any reason for this?

AR: The range of this field is very narrow anyways, so for simplicity the center point is used as input to calculate the mineral composition. We do not claim the method to be this accurate.

RC: Mineral inclusion masked from PT models because they are considered not to be part of a stable assemblage, is this justified, we see crystals f.example garnet as 'sponges' of inclusion due to seismic deformation. see Austrheim papers

AR: We did not mask mineral inclusions. We masked clasts that were not dynamically recrystallized and therefore not part of the stable assemblage.

RC: 'close to these conditions', is there a ref. for this?

AR: This is derived from the pseudosection.

RC: insufficient explanation of element maps, mineral names on fig required, what is blue in Fe in C.

AR: The initial idea of the element maps was to show the reaction of feldspar clasts and the different iron-oxide phases. We agree, that a larger map with labeled phases can be helpful for the reader.

AC: Mineral labels were added in Fig. 9.

Altenberger

RC (referee comment): The petrographic observations of the host rocks are little and sometimes not clear but these have strong relation to the conclusion
AC (author's changes to the manuscript): The petrographic descriptions of the host rock have been added and additional references provided, including a recent one by Wex et al (2017) from the same research group where the host rock conditions are considered in more detail..

RC: Are there any remnants of previous, possibly ultra-mylonitic, deformations?
AR: This was already addressed in the manuscript by clearly separating the pseudotachylytes into three categories with respect to ductile shearing– so yes, there are examples where the pseudotachylyte post-dates strong shearing. However, as visible in Fig. 3c, there are also examples of pseudotachylytes that can be found in undeformed host rocks.

RC: Are the pst concentrated in special layers of the protolithe, e-.g. involving more (OH) - bearing phases?
AR: The OH-bearing minerals are mostly limited to late- to post Musgravian intrusions. There is no affinity of pseudotachylytes to these lithologies.
AC: This has been added to the field observations.

RC: In the description of the dolerite, as a protolith, there is no given mineral assemblage (does it include grt or hbl as a (OH)-bearing phase?).
AR: The assemblage of the dolerites is "dry".
AC: The description of the paragenesis has been added to the description of sample S5.

RC: Is there any thin-section or SEM image of the mylonites adjacent to the pst (e.g. a prolongation of Fig 4).
AR: The sample of Fig. 4 is a pseudotachylyte breccia in an undeformed host rock. Examples for the ductile shearing can be found in Fig. A2 and Fig. 5a.

RC: Is the brittle deformation a direct consequence of the ductile deformation ?, e.g. same layers, or discordant after changing the stress system?
AR: Pseudotachylytes emplaced in mylonites often show localization on foliation planes, as seen for example in Fig. 3b, new Fig. 5 and Fig. A2 and in the Fig 1 of the short comment. However, the opposite can also be found as late stage pseudotachylytes crosscut the mylonitic foliation and have a somewhat random orientation.
AC: This was clarified in section 3.

RC: The reader is not informed if the minerals described are "magmatic", i.e. crystallized directly from the melt or if these are formed (overprinted) by the crustal metamorphism. In the deep crustal environment this is not easy to distinguish but has a strong impact on the interpretation. We know from some places, that kyanite can crystallize from the melt and, as it is described, the garnet with cauliflower structures are a clear evidence for rapid cooling, i.e. crystallizing directly from the melt.
AR: In the samples we used to derive the metamorphic conditions, the minerals are thought to form during dynamic recrystallization of the pseudotachylyte. In sample F44, for example, generation 1 remains unsheared and the minerals might well have crystallized directly from the melt or represent a static overgrowth of the former melt. However, the cauliflower garnet in Fig. 4 overgrows a planar foliation resulting from ductile shearing. We therefore argue that in this case the cauliflower garnet is not crystallized directly from the melt. The cauliflower garnets in the Fig. 5c however, can well be the result of direct crystallization from the melt, as they are hosted in an unsheared pseudotachylyte.

AC: Fig. 4 was extended to clearly emphasize the difference between the pseudotachylyte generations. The text was modified to clearly state whether the minerals grew from the melt, statically or by dynamic recrystallization.

RC: And how can we know, that kyanite is formed in the sample, not sillmanite? They are probably too small to distinguish by the used methods, XRD is need to confirm this, not pseudosections.
AR: Pseudosections had not been used to identify minerals in the thin sections. Kyanite was distinguished from sillimanite by using Raman spectroscopy and EBSD.
AC: This information has been added to the text.

RC: A point of interest is also: which minerals from the protolithe are consumed and which are stable. I think biotite will directly melt, producing some (OH).
AR: In the example of sample F68, biotite is slightly enriched in the pseudotachylyte. However, the amount of OH produced is small, as no new OH-bearing phases are found in the pseudotachylyte assemblage. Garnet is also readily molten, as it never appears as clasts in the pseudotachylytes. Quartz is commonly found as clasts, for example visible in Fig. 5a, where whole ribbons of quartz "survive" the melt formation. In the example of F6, most clasts are made up of plagioclase.
AC: This information was integrated into the manuscript.

RC: The descriptions of some important figures like Fig 4 is too short-and do not describe the four generations of pst sufficiently.
AC: The description of figures where enlarged, Fig. 4 was augmented with further backscatter images for all generations of pseudotachylytes.

RC: Some simple ideas have no base, if it is written, two generations of pst overprinted by ductile deformation are an indicator of cyclic brittle and ductile deformation. It is only an evidence for two phases of brittle deformation followed by ductile deformation.
AC: A new Figure 6 was added, to demonstrate the switch from brittle to ductile deformation and back to brittle. It is true, that this only represents one cycle, from brittle to ductile and back to brittle, but the chances of preservation of multiple cycles are low. In the new version of the manuscript, we avoid the use of the word "cyclic" and restrict the use of the word to the discussion part.

RC: What is the PT-conditions of the ductile deformation-any evidence? Is it possible, that the ductile event is part of the retrograde exhumation?
AR: The ductile deformation in the Davenport Shear Zone is described in detail Camacho et al. (1997), as stated in the text. As the mylonites host the sub-eclogitic assemblage, we can exclude a ductile retrograde overprint.

RC: Some parts are clearly described but not well thought: a pst in a gabbro is containing Kfs clasts - gabbros should not contain Kfs.
AR: There are no clasts of Kfs, but Pl-clasts are overgrown by Kfs.
AC: This error has been corrected in the text.

RC: I agree with the used method of pseudosections. However, is there any further indication for the deep crustal evolution, like high Al2O3 concentration in the newly formed pyroxenes, what is the composition of the melt-derived garnets-there are experimental data on the P-conditions of garnets formed from magmatic melts.
AR: The pseudotachylyte-melt derived minerals are for sure interesting in many ways, but the study of those would be beyond the scope of this publication. As garnets crystallize from the pseudotachylyte melt, they probably record the temperature of the melt, which is much higher than the ambient conditions. Al-rich pyroxenes have been described from pseudotachylytes in the Musgrave Ranges by Wenk and

Weiss (1982), and the applied barometers return pressures of about 3 GPa, thought to represent dynamic pressures, rather than lithostatic.
AC: The comment about the pyroxenes have been added to section 4.1.

RC: Therefore, please write if in the described examples recrystallization is crystallization from the melt (e.g. grt) or recrystallized under metamorphic conditions during later times from the fine-grained matrix?
AC: This has been clarified in the text.

RC: You can calculate by your data also the geothermal gradient - it is only ca 20 °/km.
AC: This information has been added to the results.

RC: However, I am wondering, that the classical paper of Handy & Bruhn (2004, EPSL,223), thinking about the cyclicity and "Stress– strain evolution for a volume of rock undergoing deformation to frictional sliding or creep at a constant slip or strain rate" is not cited.
AC: The work of Handy and Brun is now cited.

RC: The interpretations in the manuscript are not satisfying, but maybe there is no simple answer.
AR: The model of downward propagation of seismic stresses from the upper crust is favoured by many authors in recent publications, and is physically feasible but in our opinion there is no unequivocal geological evidence in previous publications that exclusively support this model. We therefore wanted to critically evaluate this model in the current study and to show the contradictions. This highlights rather than "solves" the problem and if anything provides an impetus for future studies.

RC: Is there any correlation with the drastic change in shear direction from sinsitral to dextral?
AR: The change from sinistral to dextral sense of shear is more likely the result of slight variation in orientation of the shear zones, as described in the text, as this change is lateral in space and not temporal. In some cases, shear zones do show a change in sense of shear, but no consistent change can be documented.

RC2_supplement:
RC: Nice maps, but a map of the local geology, where the samples are taken from would be of interest, too.
AR: The geological background is kept concise, therefore we did not include a geological map or profile. The geophysical maps provide a direct insight through the cover, and help to identify the main shear zones as well as the difference in metamorphic grade.
AC: We modified the text to indicate better where a geological map and cross section can be found.

RC: I would add the beautiful BSE image A 1 from the Appendix with the flow folds, which is not described in the text, yet.
AC:. We integrated the beautiful image A1 into figure 5 along with a better description.

RC2_supplement: Other comments, if not already addressed above, have been integrated in text and figures.

RC: why is it sheared? Give an evidence-
AR: There is an internal foliation visible, which is defined by garnet and biotite. This is stated in the text.

RC: And the red box is to boarder of the red box are too thin-better to do this in white
AC: The outline of the red box is now thicker.

All other comments from the supplement are discussed above. Figure captions have been enhanced to provide better insight.

Pseudotachylyte as field evidence for lower crustal earthquakes during the intracontinental Petermann Orogeny (Musgrave Block, Central Australia)

Friedrich Hawemann[1], Neil S. Mancktelow[1], Sebastian Wex[1], Alfredo Camacho[2], Giorgio Pennacchioni[3]

1 Department of Earth Sciences, ETH Zurich, Sonneggstrasse 5, CH-8092 Zurich

2 Department of Geological Sciences, University of Manitoba, 125 Dysart Rd, Winnipeg, Manitoba, R3T 2N2 Canada.

3 Department of Geosciences, University of Padova, Via Gradenigo 6, 35131 Padova, Italy

Correspondence to: Friedrich Hawemann (friedrich.hawemann@erdw.ethz.ch)

Deleted: Pennaccioni[3]

1

Abstract. Geophysical evidence for lower continental crustal earthquakes in almost all collisional orogens is in conflict with the widely accepted notion that rocks, under high grade conditions, should flow rather than fracture. Pseudotachylytes are remnants of frictional melts generated during seismic slip and can therefore be used as an indicator of former seismogenic fault zones. The Fregon Subdomain in Central Australia was deformed under dry sub-eclogitic conditions of 600-700 °C and 1.0-1.2 GPa during the intracontinental Petermann Orogeny (ca. 550 Ma) and contains abundant pseudotachylyte. These pseudotachylytes are commonly foliated, recrystallized, and crosscut by other pseudotachylytes, reflecting repeated generation during ongoing ductile deformation. This interplay is interpreted as evidence for repeated seismic brittle failure and post- to inter-seismic creep under dry lower crustal conditions. Thermodynamic modelling of the pseudotachylyte bulk composition gives the same P-T conditions of shearing as in surrounding mylonites. We conclude that pseudotachylytes in the Fregon Subdomain are a direct analogue of current seismicity in dry lower continental crust.

1 Introduction

Predicting the rheology of the Earth's crust is crucial for all geodynamic models over the whole range of length and time scales from plate tectonics to seismic hazard estimation. In general, the main constraints on rock rheology are derived from rock deformation experiments, with results obtained at high strain rates and high temperatures extrapolated to natural conditions (e.g. Kohlstedt et al., 1995). The simplest assumption of competing brittle and viscous behaviour at constant strain rate results in a typical "Christmas-tree" 1D representation of strength variation with depth (Goetze and Evans, 1979). One basic form of the strength profile for the continental lithosphere is the so-called "jelly sandwich" model, with a quartz- and feldspar-rich, wet, weak, and viscously flowing lower crust sandwiched between a strong brittle upper crust and a dry, strong, brittle upper mantle with olivine rheology (e.g. Burov and Watts, 2006; Jackson, 2002a). An alternative "crème brûlée" model considers a wet olivine rheology for the upper mantle, and therefore limits all significant strength and seismicity to the upper crust (Burov and Watts, 2006; Jackson, 2002a). However, in contradiction to such models that limit brittle deformation exclusively to the upper crust, seismicity is also recorded in the lower crust in almost all collisional settings, e.g. the Alps (Deichmann and Rybach, 1989; Singer et al., 2014), the Himalayas (Jackson, 2002b; Jackson et al., 2004), the Tien Shan (Xu et al., 2005), the central Indian shield (Rao et al., 2002), and the North Island of New Zealand (Reyners et al., 2007).

The main factors governing rock rheology are temperature, strain rate, chemical composition, water activity, and pore fluid pressure. These parameters cannot be well constrained from seismic measurements. Consequently, direct observations from field studies of exposed lower crustal sections are critical for understanding lower crustal rheology. Pseudotachylytes, generally interpreted to represent frictional melt generated during seismic failure (McKenzie and Brune, 1972; Sibson, 1975), can be locally abundant in exposures of lower crust (Altenberger et al., 2011, 2013; Austrheim and Boundy, 1994; Clarke and Norman, 1993; Moecher and Steltenpohl, 2009, 2011; Pittarello et al., 2012; Orlandini et al., 2013; Menegon et al., 2017). The metamorphic conditions of these sections correspond to depths well below the usual brittle-ductile transition zone for crustal rocks (<15 km) and thus the assumed lower limit for earthquake nucleation. Sibson (1980) reported mutually overprinting pseudotachylytes and mylonites from the Outer

64 Hebrides Thrust (NW Scotland) and similar observations were made by Moecher and Steltenpohl (2009) and Menegon
65 et al. (2017) in the Lofoten region (N Norway), by Hobbs et al. (1986) in the Redbank Shear Zone (Arunta Block,
66 Central Australia), and by Camacho et al. (1995) in the Woodroffe Thrust (Central Australia). Mutual overprinting
67 has been interpreted to reflect the generation of pseudotachylytes and mylonitization under the same conditions
68 (Altenberger et al., 2011, 2013; Clarke and Norman, 1993; Moecher and Steltenpohl, 2011; Pennacchioni and Cesare,
69 1997; Pittarello et al., 2012; Ueda et al., 2008; White, 1996, 2004, 2012). A possible explanation for the generation of
70 earthquakes in these mid- to lower crustal rocks is the downward migration of the brittle-ductile transition through the
71 transfer of stress from the upper crust after a seismic event (Ellis and Stöckhert, 2004; Handy and Brun, 2004). Another
72 mechanism for the embrittlement of the lower crust are high pore fluid pressures, and many field examples of
73 pseudotachylytes and brittle fracturing in the lower crust have been closely linked to fluid activity (Altenberger et al.,
74 2011; Austrheim et al., 1996; Lund and Austrheim, 2003; Maddock et al., 1987; Steltenpohl et al., 2006; White, 2012).
75 In contrast, Clarke and Norman (1993) considered that the preservation of fine-grained pseudotachylyte under high
76 grade conditions is only possible if the pseudotachylyte composition is dry.
77 The aim of the current study is to establish the conditions under which pseudotachylytes can form in a water deficient
78 lower crust and to demonstrate that the recurring interplay of fracture and flow represents the bulk deformation style
79 of lower crust in intracontinental settings as preserved in the Musgrave Block. The field, petrological and
80 microstructural results provide direct observational constraints on proposed models for lower crustal seismicity.

81 **2 Geological Setting**

82 The Musgrave Block in Central Australia (Fig. 1) provides excellent exposure of well-preserved lower crustal fault
83 rocks that can be studied over hundreds of kilometres (Figs. 2a,b). In this study, we focus on the Fregon Subdomain
84 in the eastern Musgrave Block, which represents the hanging wall of the Woodroffe Thrust (Camacho et al., 1997;
85 Camacho and McDougall, 2000; Wex et al., 2017).
86 The Fregon Subdomain experienced granulite facies
87 metamorphism during the Musgravian Orogeny,
88 associated with the amalgamation of the Australian
89 Cratons at about 1.2 Ga (Gray, 1978; Wade et al.,
90 2006). The voluminous Pitjantjatjara Supersuite,
91 consisting mainly of granites and charnockites, was
92 emplaced during the post-collisional stage (Smithies
93 et al., 2011). Extension at ~1070 Ma is manifested
94 by the intrusion of dolerite dykes (Alcurra Suite),
95 gabbros, and granites (Giles event; Evins et al.,
96 2010). This rift event does not seem to be associated
97 with a deformation phase in the eastern Musgrave
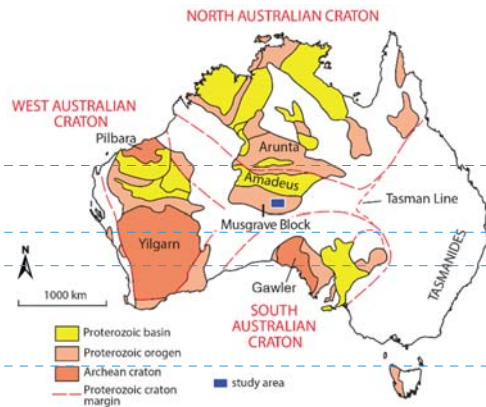98 Block, and was probably purely magmatic (Aitken

Figure 1: Position of the Musgrave Block between the Archean cratons of Australia. Modified after Evins et al. (2010).

3

et al., 2013). Another series of dolerite dykes, the Amata Suite at ca. 800 Ma, is potentially related to a mantle plume (Zhao et al., 1994). The Fregon Subdomain preserves a series of mostly strike-slip, crustal-scale shear zones developed during the Petermann Orogeny (~550 Ma; Camacho et al., 1997), all of which are associated with abundant pseudotachylytes. During the Petermann Orogeny, the Fregon Subdomain was juxtaposed against former mid-crustal rocks in the north (Mulga Park Subdomain) along the moderately to shallowly south-dipping Woodroffe Thrust (Fig. 2; Camacho et al., 1995; Major and Conor, 1993; Wex et al., 2017). The intracontinental Petermann Orogeny correlates in time with the global Pan-African Orogeny (Camacho et al., 1997) and was possibly caused by a clockwise rotation of the South and West Australian Cratons with respect to the North Australian Craton (Li and Evans, 2011). The protoliths of the Fregon and Mulga Park Subdomains are very similar in composition and age (Camacho and Fanning, 1995; Edgoose et al., 1999), but can be readily distinguished using airborne thorium (Th) concentrations as seen in Fig. 2c. The low Th concentration in the hanging wall probably relates to the formation and migration of partial melts to shallower crustal levels during the earlier granulite facies metamorphism, with the breakdown of apatite and monazite resulting in partitioning of incompatible elements, such as Th, into the melt phase (Förster and Harlov, 1999). Consequently, low Th concentrations can be used to indicate that the crust experienced granulite facies metamorphism (Lambert and Heier, 1968; Scharbert et al., 1976). The signal is partly obliterated by the granitic intrusions of the Pitjantjatjara Supersuite and Giles Event, which succeeded granulite facies metamorphism.
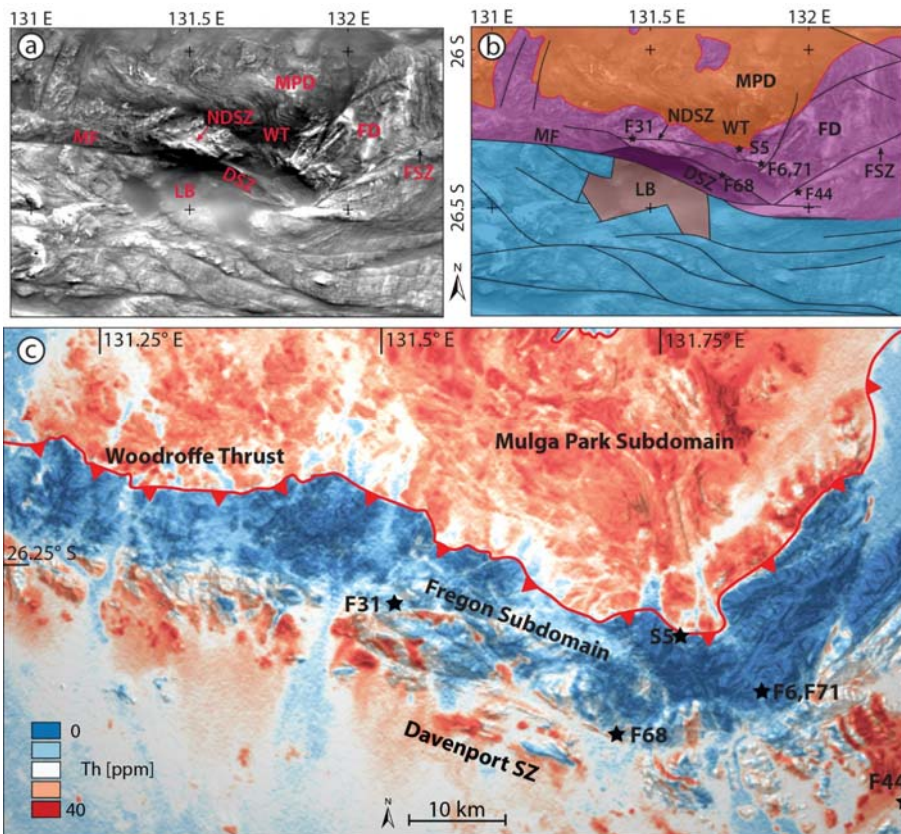
4

Figure 2: a) Total magnetic intensity map (Milligan and Nakamura, 2015) and interpreted structures. Most fault zones appear as dark lines with a marked contrast, lithological layering is visible in the Mulga Park Subdomain (MPD), whereas the sediments of the Levenger Basin (LB) appear blurred. **b)** Interpretation of the tectonic framework of the Central Musgrave Block. The Mann Fault (MF) separates units that did not experience high grade overprint during the Petermann Orogeny in the south (blue), from the Fregon Subdomain (FD, purple) in the north. The Davenport Shear Zone (DSZ), North Davenport Shear Zone (NDSZ) and the Woodroffe Thrust (WT) were mapped by integrating the magnetic intensity map with airborne imagery and direct field observations. **c)** Compilation of airborne gamma ray surveys, with concentration of thorium shown from blue (low) to red (high). Flares of low concentration in the footwall are associated with sediments transported from the hanging wall by rivers. Pseudotachylyte sample locations discussed in the text are indicated as black stars. Dataset SA_RAD_TH, Geological Survey of South Australia (2011), grey levels from hill shade. For a simplified geological map covering the same area, and an interpreted synthetic NS cross-section, see Wex et al. (2017).

5

3 Field observations

The Davenport Shear Zone (DSZ) is a strike-slip shear zone trending WNW-ESE with a sub-horizontal stretching lineation, a moderately to steeply dipping foliation (Camacho et al., 1997), and a sense of shear that changes from dominantly sinistral to dextral from west to east, reflecting the regional variation in the foliation trend. In the framework of the Musgrave Block, the DSZ is bounded to the south by the generally poorly exposed Mann Fault (Fig. 2a). While dextral strike-slip movement along the Mann Fault is indicated by the pull-apart Levenger Basin (Aitken and Betts, 2009; Camacho and McDougall, 2000), a normal, north-side up component is implied by the lack of any known high-pressure Petermann Orogeny overprint south of the Mann Fault, as inferred from the mapping work of Glikson et al. (1996), the age data of Camacho and McDougall (2000), and our own observations. To the north, deformation in the DSZ is strongly partitioned and bounded by a high-strain zone. The only continuous zone of mylonites north of the DSZ towards the Woodroffe Thrust is the coeval North Davenport Shear Zone (NDSZ) (Camacho et al., 1997). This mylonitic zone developed under similar conditions to the DSZ, but the pitch of the lineation is widely variable, from horizontal to down dip to the south, with the shear sense being dominantly dextral-oblique thrusting towards NW. The DSZ mylonites and the NDSZ converge to the west. Towards the east, the relationships are less clear because of the lack of outcrop. The ENE trending, moderately dipping Ferdinand Shear Zone is a sinistral strike-slip shear zone that appears to branch from the steep Mann Fault.

The DSZ is an approximately 5 km wide mylonitic zone with the foliation trend clearly visible on satellite images. This foliation encompasses low strain domains, from kilometre to metre scale, which potentially preserve initial stages of the temporal development of deformation. Pseudotachylytes are abundant, not only in the DSZ, but throughout the whole Fregon Subdomain. They are concentrated along, but not exclusively limited to, the different shear zones described above and especially along the Woodroffe Thrust (Camacho et al., 1995). Pseudotachylytes are easily identified in the field by their aphanitic matrix, abundance of clasts, injection veins, breccias and chilled margins (Fig. 3). When overprinted by subsequent ductile shearing, identification becomes more more difficult and cannot always be confirmed (Kirkpatrick and Rowe, 2013; Price et al., 2012). The thickness of pseudotachylyte veins reaches up to 7 cm but is usually about 1 cm. Generation surfaces, when observed, show very little former melt, as it was mostly injected into the host rock. There is no evidence for hydration, such as formation of bleached halos or hydrous mineral growth. Assemblages with significant amounts of water-bearing minerals (e.g. biotite and hornblende) are restricted to late- to post-Musgravian granitic intrusions. The pseudotachylytes do not show any specific affinity for these more hydrous units, but in fact occur in all lithologies. In all the different mylonitic shear zones of the Fregon Subdomain, the observed relative age relationship between pseudotachylyte formation and ductile shearing in the adjacent rock covers the following range of possibilities.

(1) Pseudotachylyte post-dates shearing. The mylonitic foliation in the host rock is in general crosscut and brecciated by the pseudotachylyte (Fig. 3a), although the pseudotachylyte may also be emplaced parallel to the foliation, in some cases at the boundary to ultramylonite bands or along the rim of dolerite dykes (Fig. 3b). Pseudotachylytes occur as veins or as breccias with a black aphanitic matrix, in which fragments of the host rock show a rotated internal fabric.

6

(2) Pseudotachylyte is broadly synchronous with shearing. Pseudotachylyte veins crosscut the mylonitic foliation and are themselves foliated, as visible from elongated clasts (Fig. 3c). The stretching lineation in the pseudotachylyte is parallel to that in the surrounding mylonites. Veins and breccias can show a wide range of matrix colours, from grey to beige to caramel-coloured.

(3) The pseudotachylyte itself is foliated but occurs in effectively unsheared rocks, with ductile deformation confined to the pseudotachylyte vein, while the adjacent rock remained little deformed (Figs. 3d, 4).
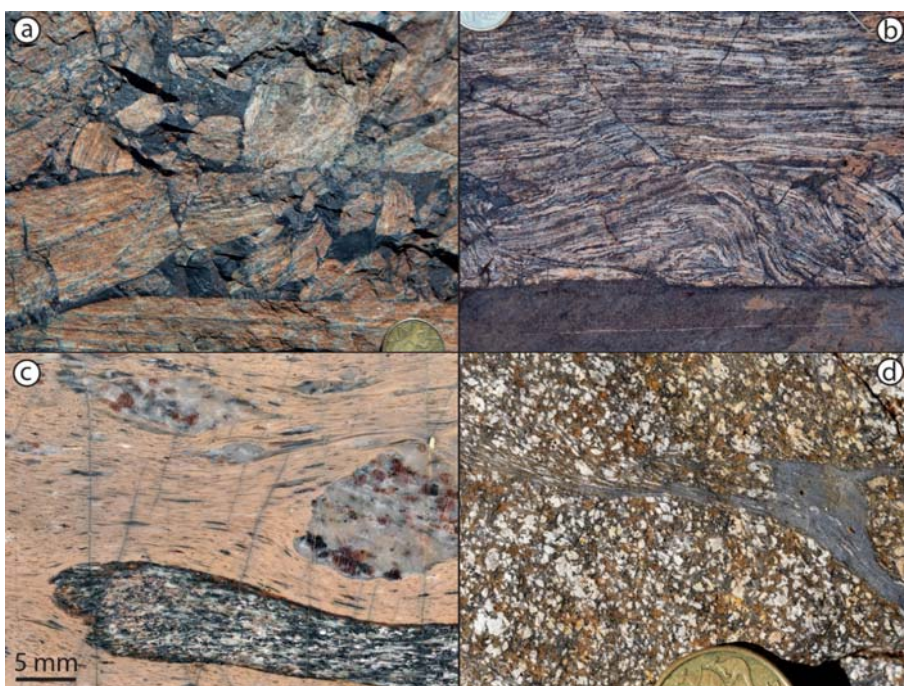
Figure 3: Field examples of pseudotachylytes: (a) Pseudotachylyte breccia disrupting mylonitic foliation. Note the relative rotation of clasts, their generally angular shape and the wide range of clast sizes. (26.3877 S, 131.7091 E). (b) Late-stage pseudotachylyte localizing at the boundary of a sheared dolerite dyke **(bottom part of the image),** creating a duplex-like structure with all planes of movement decorated by pseudotachylyte (N is up, 26.3408 S, 131.5255 E). (c) Polished slab with caramel-coloured pseudotachylyte including fragments of quartzo-feldspathic gneiss and mafic granulite. Note the internal foliation and elongation of clasts. **Note also that although the clasts are variably foliated, they are not ultramylonitic and have irregular shapes and a very wide range of sizes, typical of a cataclastic breccia (26.3853 S, 131.7105 E). (d)** Sheared pseudotachylyte **with elongated clasts** in an otherwise almost undeformed gabbro (N is up, 26.3528 S, 131.8419 E).
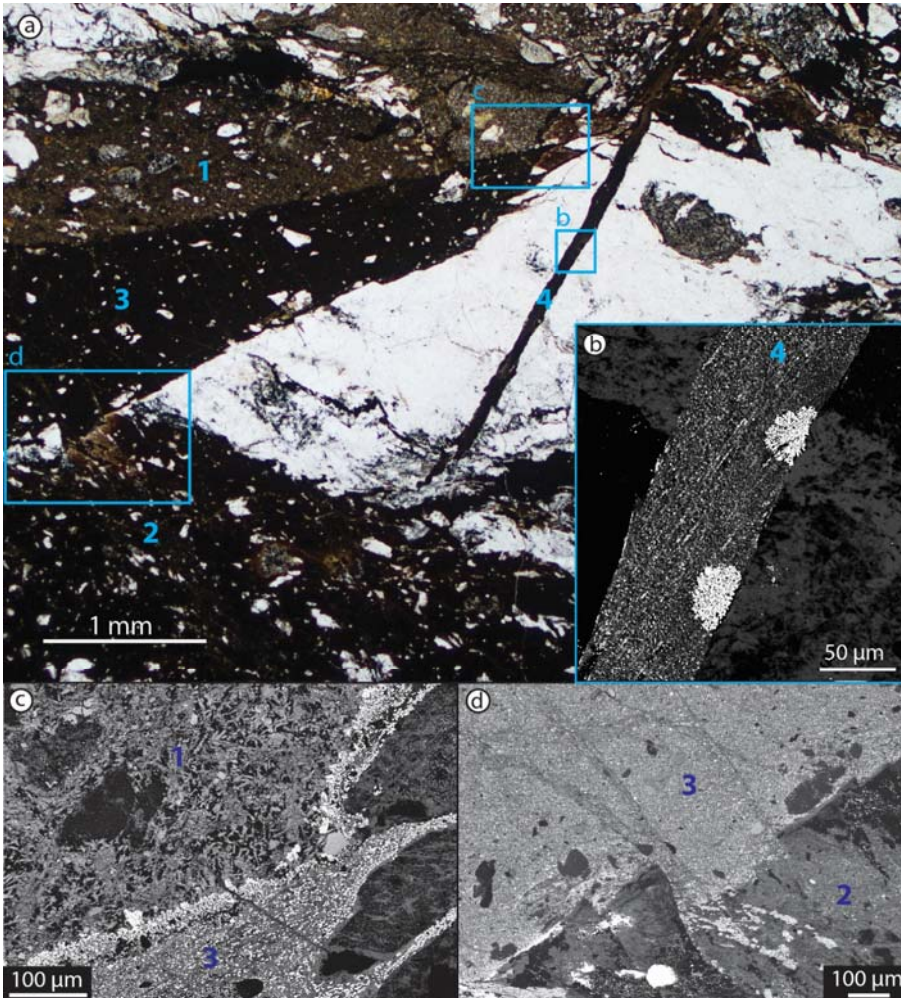
Figure 4: a) Thin section image of sample F44 (26.4514 S, 131.9553 E) showing four generations of pseudotachylyte, from oldest 1 to youngest 4 (plane polarized light; to reduce contrast, images taken with different exposure times were combined). b) Backscattered electron image of the area indicated by the blue box in (a): a vein of generation 4 shows a planar foliation, defined by elongate clasts, that is oblique to the vein boundary and is overgrown by dendritic (or "cauliflower") garnet. c) Pseudotachylyte generations 1 and 3 showing a former chilled margin now decorated by garnet. d) Pseudotachylyte generation 3 crosscutting generation 2, with the boundary offset by late fractures.

4 Microstructure

4.1 Post-shearing pseudotachylyte

Late-stage pseudotachylytes crosscut the mylonitic fabric, and show the pristine characteristic microstructures of quenched melts, preserving an extremely fine-grained matrix (grain size on the order of a few microns) with flow structures, chilled margins and angular, sometimes corroded clasts of iron oxides (Fig. 5a). In some instances, microlites of feldspar and pyroxene are observed. Since these microlites are the result of crystallization during melt undercooling, their mineral assemblages and mineral chemistry do not represent ambient temperature conditions. Al-rich pyroxenes have been described from pseudotachylytes in the Musgrave Ranges some 250 km west of the current study area by Wenk and Weiss (1982). Pressures obtained from the geobarometers applied were about 3 GPa, which the authors interpreted to represent dynamic syn-pseudotachylyte melting pressures, rather than ambient lithostatic conditions.

4.2 Syn-shearing pseudotachylyte

Sheared pseudotachylytes on occasion contain clasts of an older generation of pseudotachylyte, suggesting recurring brittle and ductile deformation. The syn-kinematic mineral assemblage of pseudotachylytes does not show any evidence for fluid infiltration.

Sample F31, located in the North Davenport Shear Zone (26.2793S, 131.4968 E), is from the immediate boundary between a garnet-bearing quartzo-feldspathic gneiss and a dolerite dyke. This contact is exploited by a pseudotachylyte (Fig. 6), which mostly incorporates the dolerite but also includes clasts of the felsic gneiss. In addition to inclusions of country rock, there are also clasts of an older generation of pseudotachylyte, strongly overprinted by ductile shear, within the breccia. Locally, the boundary of these first generation pseudotachylyte clasts is marked by a second, also sheared, generation of pseudotachylyte of greyish colour that crosscuts the older generation but is itself cut by the younger unsheared third generation (Fig. 6). These relationships demonstrate that (1) initial pseudotachylyte formation, interpreted to represent a brittle seismic event, was followed by (2) ductile shearing, followed by (3) a second seismic event, developing the grey second generation pseudotachylyte, which was then (4) again sheared, to be finally followed by (5) a third generation of unsheared pseudotachylyte and associated breccia.

Sample F68 is a garnet-bearing quartzo-feldspathic gneiss, sampled close to the northern boundary of the DSZ (same outcrop as the example in Fig. 3c; 26.3849 S, 131.7067 E). Pseudotachylyte veins are ca. 1 mm thick, spaced ca. 1 cm apart, and oriented parallel to the proto-mylonitic foliation. Pseudotachylyte veins show injections and have a fine-grained matrix of Grt+Kfs+Pl+Qz+Bt+Ky+Rt, similar to the host rock assemblage, where Ky is restricted to Pl-clasts (mineral abbreviations are after Whitney and Evans, 2010). The pseudotachylyte is slightly enriched in Bt relative to the host rock, but no other OH-bearing phases are present. Kyanite was identified by using Raman spectroscopy and EBSD. The fine grained poikilitic garnet (~20 μm, Fig. 5b) results in the caramel colour in the field (Fig. 3c). The internal foliation is defined by biotite and aggregates of garnet (Fig. 5b). In the host rock, mm-sized relict, granulite facies garnets are fractured and surrounded by smaller, neocrystallized garnet, with sizes on the order of tens of microns.

257 A sheared pseudotachylyte was sampled in the immediate hanging wall of the Woodroffe Thrust (sample S5, 26.3082
258 S, 131.7745 E), at the boundary between a sheared dolerite dyke and undeformed felsic granulite. This
259 pseudotachylyte has a paragenesis similar to the dolerite dyke (Pl+Cpx+Gt+Ky+Rt+Ilm+Qz+Kfs), but is much finer
260 grained. The boundary with the dolerite is decorated by even finer grained garnet, possibly the remnant of a chilled
261 margin with a slightly different composition. Where the pseudotachylyte injected into the granulite, it evaded shearing
262 and shows a fine-grained matrix with dendritic garnet overgrowth (Fig. 5c), possibly directly crystallizing form the
263 melt. The original flow banding is highlighted by the preferential overgrowth of garnet on some bands, probably due
264 to compositional differences (Fig. 5d).

265 **4.3 Sheared pseudotachylyte in undeformed host rock**

266 Sample F44 from the Ferdinand Shear Zone (26.3856 S, 131.9550 E) contains at least four generations of
267 pseudotachylyte veins and breccias developed in a granitic host rock (Fig. 4a-d). Individual pseudotachylyte veins
268 vary in the amount and rounding of clasts, compositional heterogeneity, and the mineral assemblage. The modal
269 abundance of Grt+Cpx+Opx+Amp+Fsp is also variable, possibly reflecting a progressive change in bulk chemistry of
270 the melt. The observed mineral assemblages in this unsheared pseudotachylyte might either be the result of
271 crystallisation directly from the melt, or later static overgrowth. Generation four clearly crosscuts older generations
272 and shows an internal foliation, which is interpreted to be the result of a ductile overprint rather than flow banding, as
273 it is nearly planar with a consistent oblique angle to the margin of the pseudotachylyte. The margin of this
274 pseudotachylyte is decorated with dendritic garnet that clearly overgrows the planar foliation (Fig. 4b), indicating
275 post-shearing high grade conditions rather than crystallization from the melt.
276 Sample F6 is a gabbro assigned to the Giles Complex (Fig. 3d; 26.3528 S, 131.8419 E), which largely preserves its
277 magmatic texture, but contains sheared pseudotachylyte. The host rock is almost undeformed and shows static
278 reactions such as Grt coronas around Pl in contact with Cpx and breakdown of Opx and Pl to Cpx. The pseudotachylyte
279 contains a large number of clasts (ca. 50% of the total volume), dominantly of Pl, which show limited recrystallization.
280 The matrix minerals of the dynamically recrystallized pseudotachylyte consists of
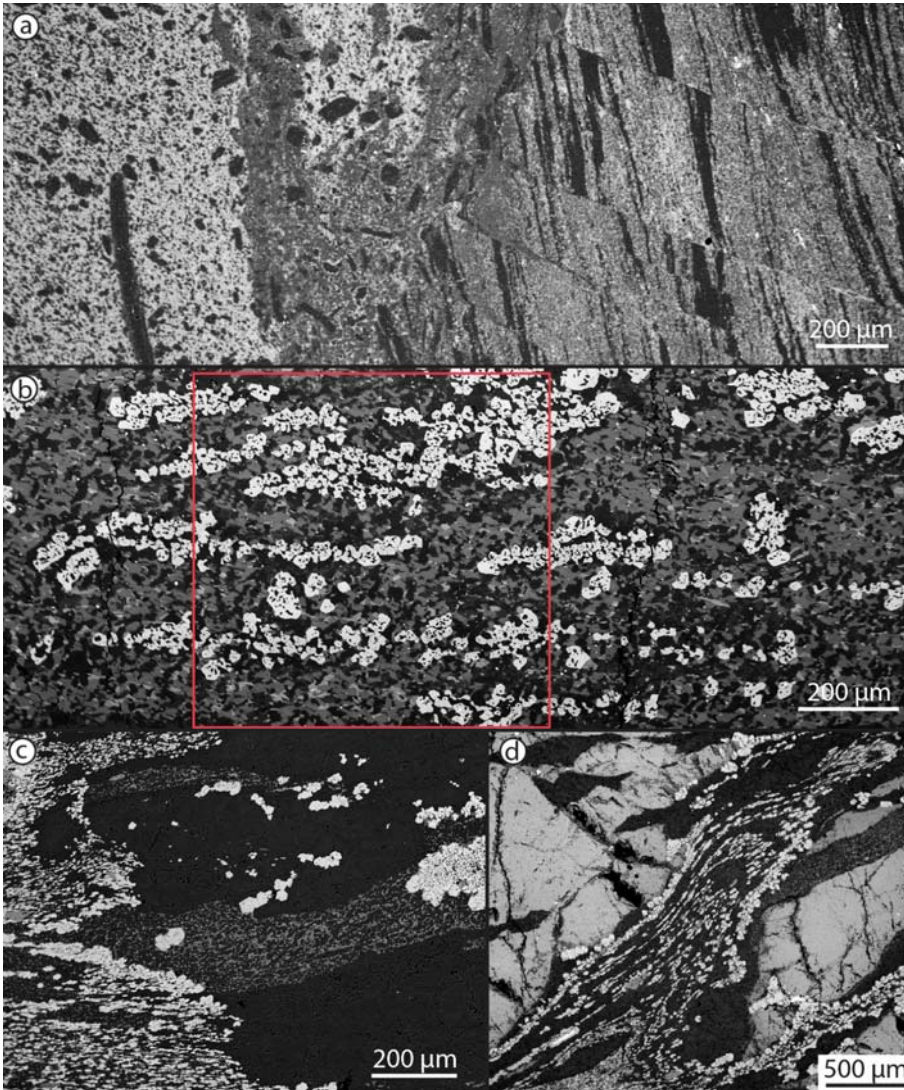281 Grt+Cpx+Kfs+Qz+Mag+Rt+Ilm+Ky.

Figure 5: Backscattered electron images of pseudotachylyte: (a) Late-stage pseudotachylyte with angular clasts in mylonitic host rock with abundant fractures (26.3550 S, 131.8432 E). (b) Dynamically recrystallized pseudotachylyte in sample F68. Minerals in greyscale from dark to bright are Qz, Pl, Kfs, Ky, Bt, Grt. Red box indicates the mapped area for Fig. 7. (c) Unsheared pseudotachylyte in a vein cutting through a plagioclase grain of the granulitic host rock showing dendritic overgrowth of garnet. In the left part of the image, the pseudotachylyte is fine grained and foliated (sample S5). d) Injection vein preserves original flow banding, visible through the selective overgrowth of garnet (sample S5).

303

11
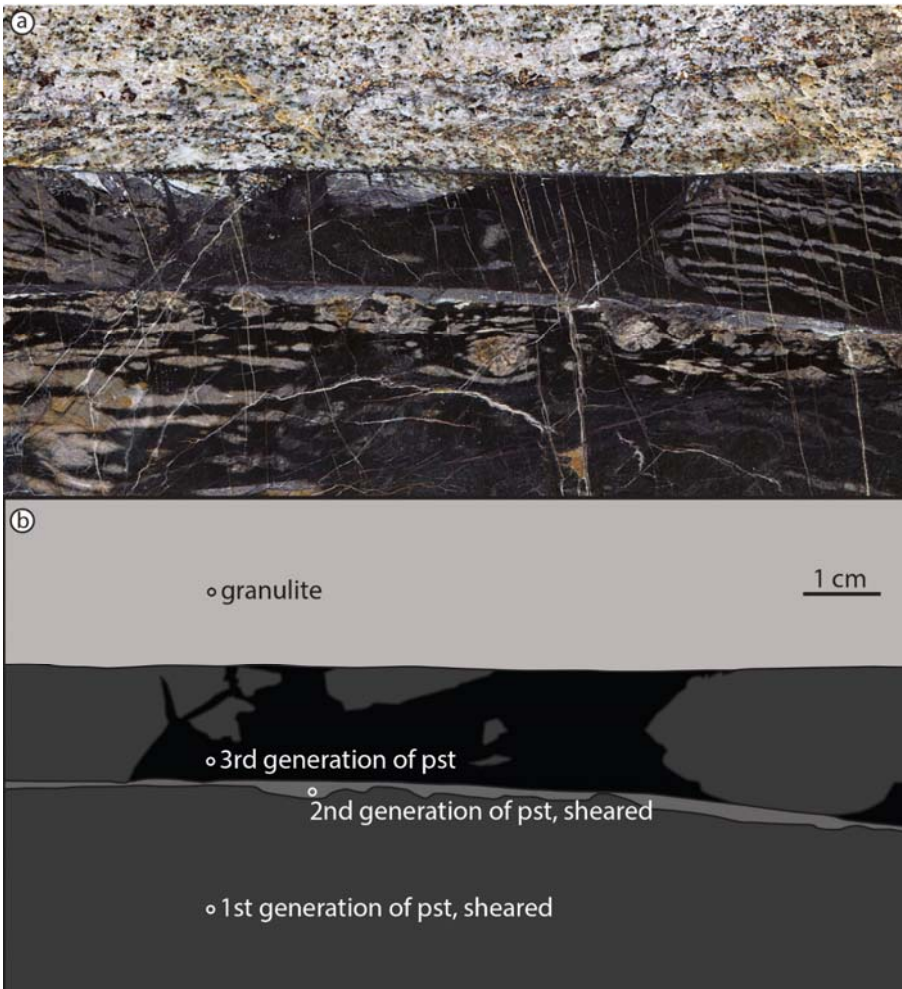
304

Figure 6: a) Scan of a polished rock slab (sample F31; 26.2793S, 131.4968 E), and b) sketch of the same area. The sample shows three generations of pseudotachylyte, developed at the boundary between garnet-bearing quartzo-feldspathic gneiss (to the top) and a dolerite dyke (below and outside the image). The first generation of pseudotachylyte contains clasts of the quartzo-feldspathic host (upper part of the image), which are intensively sheared. This generation is crosscut by a second generation of pseudotachylyte, which is present as a light grey vein, with much smaller clasts, which are also elongated. The third generation of pseudotachylyte exhibits a sharp boundary to the host rock in the upper part of the image and incorporates clasts of the first generation pseudotachylyte.

5 Conditions of pseudotachylyte emplacement

5.1 Methods

Backscattered electron (BSE) images were taken with a FEI Quanta 200F scanning electron microscope, equipped with a field emission gun deployed at the ScopeM (Scientific Center for Optical and Electron Microscopy, ETH Zurich). Quantitative measurements of mineral composition were acquired with a JEOL JXA-8200 electron probe micro analyser (EPMA) at the Institute for Geochemistry and Petrology, ETH Zurich, with a set of natural standards. Voltage was reduced from 15 kV to 10 kV for some samples to account for the fine grain size. Thermodynamic modelling using Perple_X (Connolly, 1990) was carried out on three samples of recrystallized pseudotachylytes within different host rocks. The determination of a bulk composition for pseudotachylytes by using the classic XRF-method (X-Ray Fluorescence) is hampered by their geometry and the presence of abundant clasts (Di Toro and Pennacchioni, 2004). To minimize these problems, the Matlab toolbox XMapTools (Lanari et al., 2014) was used to calculate the bulk composition from WDS-maps (wavelength dispersive spectrometer) collected with the EPMA. Quantitative point analysis was used to "standardize" the maps (Lanari et al., 2014). Here, the weight per cent (wt%) of a point analysis is linked to counts for each element of the same point on the map. This can be done for each mineral phase separately to account for matrix effects. After correlating the counts to wt% of all pixels, the bulk composition of the pseudotachylyte for the desired area of the map was extracted and used as input for Perple_X. For all samples, a standardization for each separate mineral was impossible because of the fine grain size. Instead, all count values on the map were correlated to a mean wt% value from point analysis. The resulting deviation in mineral chemistry is generally low and was corrected manually by comparing exported compositions from the standardized maps with measured analyses. The bias on the bulk composition induced by the choice of area can be tested by using a Monte Carlo approach (integrated in XMapTools). The deviations in wt% are in the order of 0.4 for silica and much lower for the other elements. The thermodynamic dataset of Holland and Powell (1998) was used to calculate pseudosections for the composition of the samples and a range of P-T-conditions to compare with the observed assemblage in dynamically recrystallized pseudotachylyte. The solution models used can be found in the appendix (Tables B1-3).

5.2 Results

5.2.1 Syn-shearing pseudotachylyte

The pseudotachylyte veins in sample F68 have a homogeneous phase distribution with a relatively large grain size (~20 μm), and are almost devoid of clasts (Fig. 5b). The compositional (WDS) map, which was used for calculation of a pseudosection (Fig. 7), has a size of 400x400 pixels and measurements were made using a step size of 2 μm, resulting in an area of 0.64 mm^2. The amount of water in the rock could not be measured directly, and was calculated

13

347 using an assumption of 3 wt% water in biotite and its modal
348 abundance, since biotite is the only OH-bearing mineral. As
349 biotite is a platy mineral, its area in the section parallel to the
350 lineation and perpendicular to the foliation might be under-
351 represented. However, an arbitrary threefold increase of bulk
352 water content in the calculations (from 0.05 to 0.15 wt%)
353 does not have a noticeable effect on the stability fields of the
354 mineral phases. The stability field for the assemblage of the
355 recrystallized pseudotachylyte in sample F68 is wide, which
356 is why pressure-temperature (P-T) conditions were further
357 delimited with mineral isopleths (Fig. 7). The conditions
358 estimated are around 1.05 GPa and 600 °C. The
359 stoichiometry for each mineral can be reliably reproduced
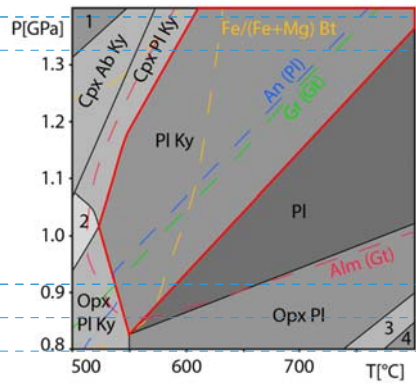360 (Table B1).

Figure 7: Pseudosection calculated for F68. Additional phases in all fields: Kfs+Grt+Bt+Qz+Rt. With isopleths for Fe/(Fe+Mg) in biotite, anorthite component of plagioclase (An (Pl)), grossular and almandine component of garnet (Gr, Alm (Gt)). Numbered Fields: 1: Cpx, Ky; 2: Opx, Cpx, Pl, Ky; 3: Opx, Pl, Ilm; 4: Opx, Pl, Ilm, no Rt

361 In sample S5, the pseudotachylyte shows strong
362 compositional heterogeneity parallel to the foliation,
363 probably due to differences associated with original flow
364 banding. This is best visible in the Ca-compositional map of Fig. 8a, where areas 1 and 2 show lower Ca-content in
365 Pl with respect to the other areas. Areas 1, 2 and 3 have a similar paragenesis of Grt+Cpx+Pl+Kfs+Rt, with Qz limited
366 to area 2, while area 3 also lacks Kfs. Areas 4 and 5 consist of Grt+Cpx+Pl+Bt+Opx+Rt. A bulk composition was
367 calculated individually for each area. Clasts of Ca-rich Pl are present (see upper right corner of 7a for an example),
368 with Ky needles growing inside the clasts but not in the matrix assemblage. These Pl-clasts were masked out for the
369 calculation of the local bulk composition since they are not part of the stable assemblage. Calculated pseudosections
370 for each area were superimposed onto each other to narrow down the P-T estimates of coeval formation (Fig. 8b).
371 Area 4 was not considered, since modelling predicted sapphirine to be stable, which was not observed in the sample.
372 Otherwise, the stable assemblage field for area 4 overlaps largely with those of the other areas. The stability of Opx
373 with the bulk compositions of areas 4 and 5 is limited to a maximum pressure of about 0.8 GPa. Since Opx occurs as
374 coronas around Cpx, we assume that Opx-growth is post-kinematic (see area 5 in Fig. 8a, where Opx appears as small
375 dark blue dots around the Cpx). Therefore, Opx was not considered to be stable in the sheared paragenesis of area 5.
376 The pseudosections show an overlap of the different stable parageneses for their respective local bulk composition
377 (Fig. 8b). The shared stability field spans the range 1.1-1.3 GPa and 670-710 °C. The compositions of individual
378 phases derived from the Perple_X model, calculated at 1.2 GPa and 690 °C, are in good agreement with the measured
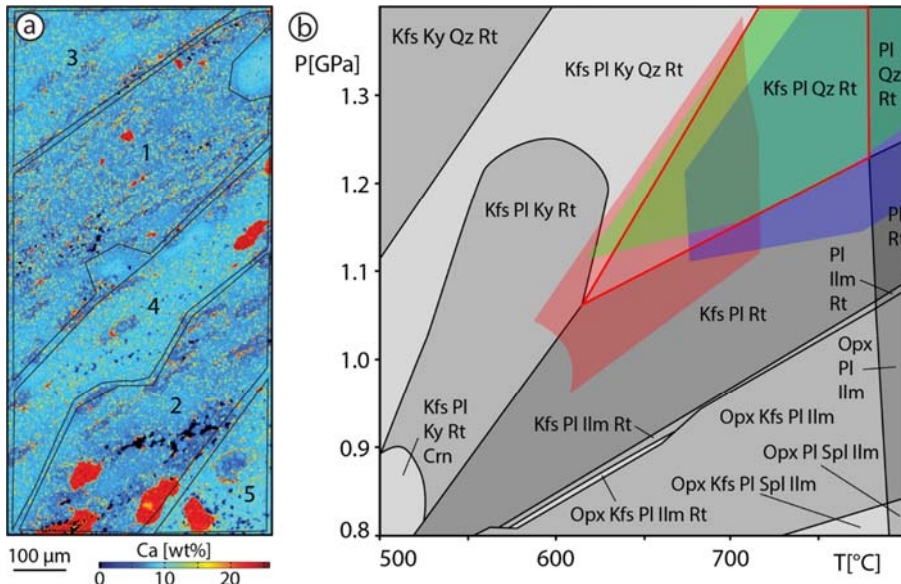379 compositions (Table B2).

Figure 8: **Quantified X-ray map for Ca for sample S5 with a step size of 2 μm and 250x500 pixels. Minerals visible: red: Cpx, dark blue: Grt, medium blue: low-Ca Pl, light blue: high-Ca Pl. Areas are defined by the Pl-composition. b) Pseudosection for sample S5, area 2; all parageneses also have Grt+Cpx. Overlays of the observed stability fields for parageneses from pseudosections from the other areas: red: area 1, green: area 3, blue: area 5. For the microstructural context of the area, see Fig. A1.**

5.2.2 Sheared pseudotachylyte in undeformed host rock

Pseudotachylyte in the gabbroic sample (F6) is extremely fine grained and is dominated by millimetre-sized clasts of Pl, which only partly reacted to form Grt and Kfs. The compositional (EDS) map was collected with a step size of 1 μm and 400x500 pixels, to account for the small grain size. The area is located between a remnant Pl-clast, overgrown by Grt with the rim replaced by Kfs, and a ribbon of mixed Kfs and Pl (Figs. 9a,c). The area in between, with abundant Grt+Ap+Mag, is interpreted to have directly originated from the former pseudotachylyte melt and recrystallized during shearing. Smaller Fsp-clasts were masked out during determination of the local bulk composition because reactions and mixing seem to be incomplete. Apatite was removed completely for the calculation of the composition, as P was not measured nor integrated into the modelling. The high content of Fe^{3+}-bearing minerals, such as Ilm and Mag (Fig. 9c), required that the Fe^{2+}/Fe^{3+} ratio to be calculated using the volume per cent of each iron-bearing phase and their respective Fe^{2+}/Fe^{3+} ratio. The calculated pseudosection (Fig. 9b) shows a narrow area for the observed assemblage of Grt+Cpx+Kfs+Qz+Ilm+Rt+Mag+Ky at conditions of ca. 1.23 GPa and 590 °C. Rt only appears as exsolution lamellae from the Ti-rich Ilm, which is a reaction taking place close to the P-T conditions derived from pseudosection modelling. Initial calculations were done with the Cpx solution model used for the other samples, resulting in lower

15

428 pressures (ca. 1.15 GPa), but predicted much higher Na-content in the Cpx of 6.5 wt% compared to the measured 2

429 wt%. The Cpx-model used for the final calculations yields compositions much closer to those measured (Table B3).

430

431
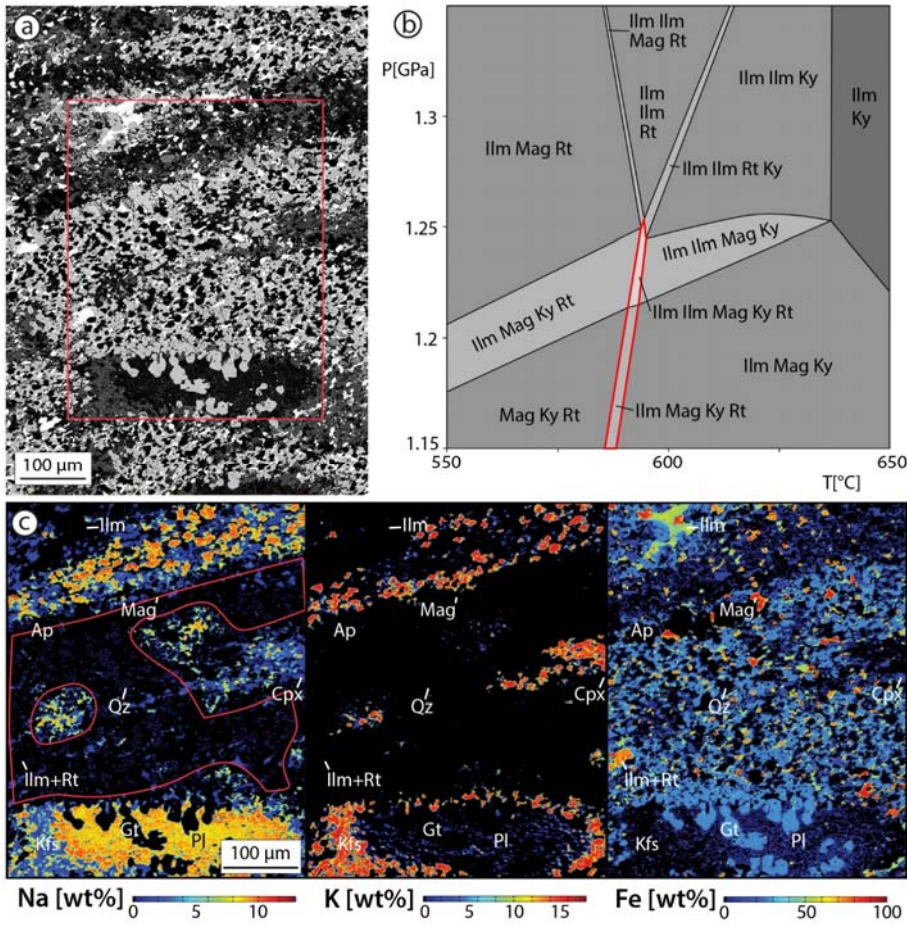
Figure 9: a) BSE image of a sheared pseudotachylyte with partly recrystallized clasts. Red box indicates the location of the X-ray-map. b) Results from thermodynamic modelling using Perple_X with an estimate for the conditions of shearing at about 1.23 GPa and 590 °C. Minerals stable in all fields: Grt, Cpx, Kfs, Qz. c) Compilation of X-ray maps: Na-map shows the incomplete breakdown of a Pl-clasts in the bottom of the image and the replacement with Kfs (K-map). Red outline shows the extracted area of the bulk composition used. Fe-map shows abundant Mag (red) and two distinct Ilm populations (green and yellow).

Deleted: :

Deleted: orange

16

6 Summary

Multiple crosscutting sheared pseudotachylytes can be interpreted as a repeated interplay between brittle and ductile deformation. As a general observation, alternating seismic fracture and aseismic creep could potentially involve even more cycles, but it becomes increasingly difficult to demonstrate, because periods of accumulated shear strain localized on the pseudotachylyte zones tend to obscure earlier crosscutting relationships. Based on this clear evidence for repeated interplay, the pressure and temperature conditions derived from the dynamically recrystallized assemblage of sheared pseudotachylyte are interpreted to be close to the ambient host rock conditions of pseudotachylyte formation and injection. Thermodynamic modelling results yield values of 1.0-1.3 GPa and 600-700 °C. These results are very similar to the estimated conditions of mylonitisation in the Fregon Subdomain during the Petermann Orogeny of 650 °C and 1.2 GPa (Ellis & Maboko, 1992; Camacho et al., 1997). Such metamorphic conditions during the Petermann Orogeny imply an average geothermal gradient of ca. 16-18 °C/km for the studied rocks, as already noted by Camacho et al. (1997) and Wex et al. (2017) in the current area and by Scrimgeour and Close (1999) in the Mann Ranges further to the west. These values are low in comparison to those typical of collisional orogens and are more characteristic of cratonic continental crust (Sclater et al., 1980). Indeed, as discussed by Wex et al. (2017), measured heat flow values in region of the Musgrave Block would imply similar values for the geothermal gradient in the middle to lower crust today.

Lin et al., (2005) described pseudotachylytes in the hanging wall of the Woodroffe Thrust and interpreted them to have been generated during Musgravian Orogeny granulite facies metamorphism. This interpretation can be ruled out for two main reasons: 1) The hanging wall of the Woodroffe Thrust experienced granulite facies metamorphism during the ca. 1.2 Ga Musgravian Orogeny but all pseudotachylytes observed in the field and described in Lin (2005) are associated with structures related to the ca. 550 Ma Petermann Orogeny. 2) Pseudotachylytes are present in gabbros (Fig. 3d) and dolerite dykes (Fig. 3b) that intruded during the ca. 1.07 Ga Giles Event and dolerite dykes of the ca. 800 Ma Amata Suite. All these magmatic rocks were intruded well after the granulite facies metamorphism associated with the Musgravian Orogeny.

7 Discussion

Pseudotachylyte development by brittle failure and frictional seismic slip (McKenzie and Brune, 1972; Sibson, 1975) is the favoured mechanism to explain the field observations in the Fregon Subdomain. Alternative processes involving thermal runaway during ductile shear (John et al., 2009; Thielmann et al., 2015) or ductile instabilities (Hobbs et al., 1986) require that a pseudotachylyte-bearing fault necessarily had a ductile precursor. This is not in accord with the observation that many pseudotachylytes occur in otherwise unsheared host rocks and act as a precursor for subsequent ductile shearing, rather than the other way around. In addition, pseudotachylytes within undeformed host rock do not necessarily contain clasts of mylonites and especially not clasts of ultramylonites. The clasts in pseudotachylytes are also typically angular and show a very wide size range (Figs. 3-6), which is consistent with fracture and brecciation. As discussed above, there can be repeated cycles of pseudotachylyte formation and shearing, with the result that clasts of sheared pseudotachylyte are included in later pseudotachylyte. This very fine grained, sheared material is preserved

17

and not totally consumed by melting. It cannot therefore, be argued that all evidence for a precursor ultramylonitic zone is lost because the ultramylonite is always totally melted during subsequent "self-localizing thermal runaway" (John et al, 2009). We would argue that examples such as shown in Fig. 6, where the pseudotachylyte zone discretely crosscuts an older granulite facies foliation at a low angle without any evidence for crystal-plastic shearing, is best explained by seismic fracture and pseudotachylyte development by frictional melting. Furthermore, fractured garnet is potentially an indicator for seismic stresses (Trepmann and Stöckhert, 2002) and has been reported to occur specifically in close association with pseudotachylytes (Austrheim et al., 2017). However, in the area of the current study, fracturing of older granulite facies garnet is widespread and not limited to the immediate border of pseudotachylytes.

Brittle deformation under elevated temperatures at depths below the classic brittle-ductile transition zone in felsic continental crust might be explained by local high fluid pressure promoting fracturing (Altenberger et al., 2011; Lund and Austrheim, 2003; Steltenpohl et al., 2006; White, 2012), either due to dehydration reactions or fluid infiltration. However, these mechanisms can be excluded for the examples presented here, because most host rocks (in particular the felsic granulites) were already thoroughly dehydrated during the earlier granulite facies Musgravian Orogeny and there is no evidence for fluid infiltration during the Petermann Orogeny. As seen for example in sample S5, the hydrous mineral biotite is restricted to isolated domains, indicating that the activity of OH was low. The absence of hydration associated with pseudotachylyte development in the shear zones described here also indicates that the switch between seismic brittle fracture (pseudotachylyte) and ductile shearing was not induced by infiltration of fluids. This is in marked contrast to what has been previously described in the Bergen Arc (Austrheim, 2013, and references therein) and Lofoten area (Menegon et al., 2017) of Norway, where fluid influx promoted by propagation of the earthquake fracture and associated weakening due to metamorphic reaction localized subsequent ductile shearing. In the absence of elevated pore fluid pressure, high stresses are necessary to fracture rocks under dry, lower crustal conditions (Sibson and Toy, 2006; Menegon et al, 2017). Natural examples of shear zones with small grain sizes developed under amphibolite facies conditions suggest that mid- and lower crust can be strong (Fitz Gerald et al., 2006; Menegon et al., 2011). This might explain initial fracturing, but on the long term, shear zones show localization of strain and therefore indicate weakening of the rocks. To explain the observed cyclicity of fracture and flow, temporal stress variations are necessary. Transient high stresses in the mid- to lower crust have been proposed to result from a downward propagation of stresses from the usual seismogenic zone (<15 km) during seismic failure (Ellis and Stöckhert, 2004a; Handy and Brun, 2004; Moecher and Steltenpohl, 2009). In the example of the 2015 Gorkha earthquake on the Main Himalayan Thrust (Duputel et al., 2016), there are indeed aftershocks located in the deeper crust following an earthquake at about 15 km depth. Alternatively, for a "jelly-sandwich" style lithospheric model, stress propagating upwards from the seismogenic zone in the strong upper mantle could also explain lower crustal seismicity. Both of these options are hard to test from field observations. However, the implication of these conceptual models is that for each event recorded in the lower crust (> 30 km depth), such as the pseudotachylytes in the Davenport Shear Zone, there was necessarily a large earthquake with a source in the upper crust or upper mantle. However, this is not observed for many large, lower crustal earthquakes, for example in the Indian Shield (Mitra et

18

534 al., 2004). Considering the abundance of pseudotachylytes in the lower crustal Fregon Subdomain, this would imply
535 a correspondingly large and perhaps unrealistic amount of strong seismicity in the upper crust or upper mantle
536 respectively, suggesting that such localized pseudotachylytes may have had a local trigger in the dry lower continental
537 crust.

8 Conclusions

539 The Fregon Subdomain documents seismic fracturing under lower crustal conditions of about 1.0-1.3 GPa and 600-
540 700 °C in an intracontinental setting. Repeated episodes of brittle failure and ductile creep represent recurring
541 earthquake cycles and a strong variation of stress in a water-deficient lower crust. It is questionable whether current
542 models of downward propagation of seismic stresses from the "seismogenic" upper crust can explain the observed
543 repetition of brittle failure and ductile shearing sporadically distributed over such a wide area. It seems more likely
544 that these earthquake cycles are locally triggered in the dry lower continental crust, at least in this intracontinental
545 setting. Models should therefore take into account temporal and spatial variations of stress in a heterogeneously
546 deforming lower crust.

Appendix A, additional images
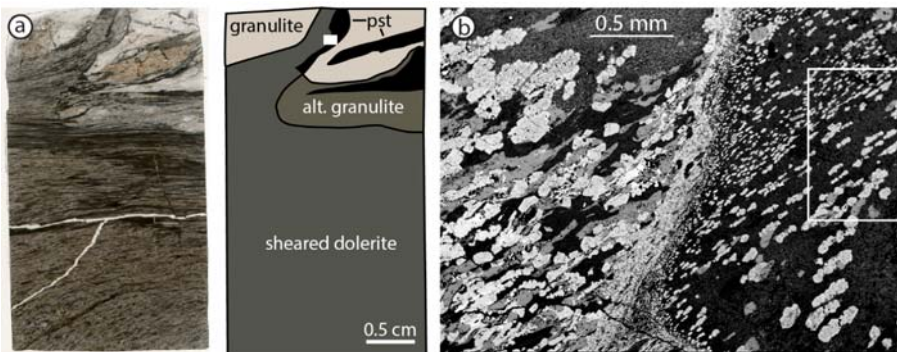
548 **Figure A1:** Microstructural context of area mapped in sample S5 (Fig. 8): a) Plane polarized light microscopic image and
549 sketch of the thin section, with box indicating image in b). b) BSE image of the boundary between dolerite (left) and sheared
550 pseudotachylyte, with the white box indicating area in Fig. 8a.

19

Appendix B, Bulk and mineral chemistry

	Bulk	Grt_m	Grt_c	Pl_m	Pl_c	Kfs	Kfs_c	Ky_m	Ky_c	Bt_m	Bt_c
Na_2O	1.06	0.02	0.00	8.77	8.14	0.89	1.33	0.00	0.00	0.19	0.00
MgO	2.67	8.31	9.28	0.01	0.00	0.00	0.00	0.00	0.00	19.04	18.56
Al_2O_3	12.76	22.61	22.30	21.93	24.20	18.92	18.56	62.40	62.92	14.73	17.67
SiO_2	70.2	38.55	39.42	58.69	61.49	63.10	65.08	36.66	37.08	37.61	37.61
K_2O	3.77	0.02	0.00	0.19	0.55	15.53	14.91	0.00	0.00	10.19	10.76
CaO	1.98	5.83	5.63	5.40	5.61	0.05	0.12	0.03	0.00	0.01	0.00
TiO_2	0.79	0.08	0.00	0.04	0.00	0.01	0.00	0.04	0.00	3.97	4.75
MnO	0.23	0.92	0.88	0.01	0.00	0.00	0.00	0.05	0.00	0.00	0.01
FeO	5.85	23.72	22.48	0.11	0.00	0.19	0.00	1.12	0.00	7.36	7.60
H_2O	0.05*									3**	3.04
total	99.31	100.06	100.00	95.15	99.99	98.69	100.00	100.29	100.00	96.10	100.00
Cations											
Al		2.04	2.00	1.21	1.26	1.04	1.01	1.99	2.00	1.29	1.48
Si		2.96	3.00	2.75	2.73	2.94	2.99	0.99	1.00	2.79	2.68
		5.00	5.00	3.96	3.99	3.98	4.00	2.98	3.00	4.08	4.16
Fe		1.52	1.43							0.46	0.45
Mg		0.95	1.05							2.11	1.97
Mn		0.06	0.06								
Ca		0.48	0.46	0.27	0.27	0.00	0.01				
Na				0.80	0.70	0.08	0.12				
K				0.01	0.03	0.92	0.87			0.96	0.98
total		3.01	3.00	1.07	1.00	1.00	1.00			3.53	3.40

Table B1: Representative analysis for sample F68. m=measured; c=calculated from Perple_X at 1.2 GPa and 690 °C; *calculated: volume per cent Bt and 3 weight per cent water in Bt; **assumed; Solution models: Omph(GHP), GlTrTsPg, melt(HP), Chl(HP), Sp(HP), Gt(GCT), Opx(HP), Mica(CHA1), Ctd(HP), St(HP), Bio(TCC), hCrd, Osm(HP), Carp(HP), Sud, feldspar, IlGkPy, Neph(FB), Chum

Deleted: A3

Deleted: perplex

	Area 1	Area 2	Area 3	Area 4	Area 5	Grt_m	Grt_c	Pl_m	Pl_c	Kfs_m	Kfs_c	Cpx_m	Cpx_c
Na_2O	4.42	3.89	5.59	5.60	4.72	0.00	0.00	6.71	6.97	0.19	1.47	1.23	1.47
MgO	4.79	5.37	2.56	2.44	4.16	11.52	11.25	0.06	0.00	0.09	0.00	15.71	15.05
Al_2O_3	21.00	21.15	23.50	23.87	22.33	23.41	22.71	25.97	25.62	19.01	18.72	3.76	2.42
SiO_2	52.30	52.04	54.99	55.45	53.85	40.16	40.14	59.33	59.30	64.04	64.94	51.85	55.20
K_2O	0.58	0.71	0.42	0.47	0.49	0.01	0.00	0.28	0.82	14.29	14.58	0.01	0.00
CaO	8.76	9.02	8.76	9.58	10.12	7.26	7.26	7.44	7.30	0.17	0.29	22.25	23.10
TiO_2	0.41	0.36	0.38	0.35	0.33	0.03	0.00	0.10	0.00	0.04	0.00	0.20	0.00
MnO	0.15	0.16	0.12	0.11	0.12	0.35	0.52	0.01	0.00	0.00	0.00	0.02	0.00
FeO	5.12	5.92	2.30	1.13	2.47	18.17	18.12	0.13	0.00	0.45	0.00	3.75	2.78
H_2O	0.00	0.00	0.00	0.00	0.00								
total	97.53	98.62	98.62	99.00	98.58	100.91	100.00	100.02	100.00	98.28	100.00	98.78	100.00

Cations													
Al						2.04	2.00	1.36	1.35	1.04	1.01	0.16	0.10
Si						2.97	3.00	2.64	2.65	2.98	2.99	1.92	2.00
						5.01	5.00	4.01	4.00	4.03	4.00		
Fe						1.12	1.13					0.12	0.08
Mg						1.27	1.25					0.87	0.81
Mn						0.02	0.03					0.00	0
Ca						0.58	0.58	0.36	0.35	0.01	0.01	0.88	0.90
Na								0.58	0.60	0.02	0.13	0.09	0.10
K								0.02	0.05	0.85	0.85	0.00	0.00
total						2.99	3.00	0.95	1.00	0.87	1.00	1.95	1.90

Table B2: Representative analysis for sample S5. m=measured; c=calculated from Perple_X at 1.2 GPa and 690 °C, all mineral chemistry from area 2; Solution models: Omph(GHP), GlTrTsPg, melt(HP), Chl(HP), Sp(HP), Gt(GCT), Opx(HP), Mica(CHA1), Ctd(HP), St(HP), Bio(TCC), hCrd, Osm(HP), Carp(HP), Sud, feldspar, IlGkPy, Neph(FB), Chum

Deleted: perplex

	Bulk	Gt_m	Gt_c	Kfs_m	Kfs_c	Cpx_m	Cpx_c
Na_2O	0.17	0.01	0.00	0.67	0.10	1.99	2.35
MgO	3.76	6.27	5.90	0.04	0.00	11.96	10.18
Al_2O_3	11.75	21.88	21.31	19.54	18.36	4.02	6.76
SiO_2	53.22	38.79	38.54	62.81	64.75	52.46	49.90
K_2O	0.04	0.00	0.00	15.97	16.75	0.03	0.00
CaO	5.09	6.64	7.35	0.08	0.04	20.15	20.88
TiO_2	3.24	0.10	0.00	0.04	0.00	0.25	0.00
MnO	0.38	0.92	0.82	0.01	0.00	0.09	0.00
FeO	14.90	26.43	25.37	0.69	0.00	9.07	3.84
Fe_2O_3	7.87		0.77				6.08
H_2O	0.00						
total	100.41	101.04	100.05	99.84	100.00	100.01	99.99
Cations							
Al		1.99	1.96	1.07	1.00	0.18	0.30
Si		2.99	3.00	2.93	3.00	1.95	1.87
		4.98	4.96	4.00	4.00		
Fe		1.70	1.70			0.28	0.31
Mg		0.72	0.69			0.66	0.57
Mn		0.06	0.05				
Ca		0.55	0.61	0.00	0.00	0.80	0.84
Na				0.06	0.01	0.14	0.17
K				0.95	0.99		
total		3.03	3.05	1.01	1.00	1.89	1.89

573 **Table B3: Representative analysis for sample F6. m=measured; c=calculated from Perple_X at 1.17 GPa and 590 °C; Fe_2O_3**
574 **calculated on the basis of volume per cent of phases; Solution models Gt(WPH), IlHm(A), MtUl(A), Omph(HP), GlTrTsPg,**
575 **melt(HP), Chl(HP), Sp(HP), Opx(HP), Mica(CHA1), Ctd(HP), St(HP), Bio(TCC), hCrd Sapp(HP), Osm(HP), Carp(HP),**
576 **Sud, feldspar, Neph(FB)**

577

578 **Appendix C**

S5	26.3082 S, 131.7745 E
F6	26.3528 S, 131.8419 E
F31	26.2793S, 131.4968 E
F44	26.4514 S, 131.9553 E
F68	26.3849 S, 131.7067 E
F71	26.3550 S, 131.8432 E

579 **Table C1 Summary of coordinates (WGS 84) of sample locations discussed in the text.**

580

Author contribution

All authors listed took part in at least two of the three field seasons, which formed the basis of this study. AC's previous knowledge of the field area and the local people was essential for the success of the campaign. SW contributed to the microprobe work. NM and GP developed the initial idea of the study and the project was financed by a Swiss National Science Foundation (SNF) Grant awarded to NM. FH prepared the manuscript with contributions from all co-authors.

References

Aitken, A. and Betts, P.: Constraints on the Proterozoic supercontinent cycle from the structural evolution of the south-central Musgrave Province, central Australia, Precambrian Research, 168(3–4), 284–300, doi:10.1016/j.precamres.2008.10.006, 2009.

Aitken, A. R. A., Smithies, R. H., Dentith, M. C., Joly, A., Evans, S. and Howard, H. M.: Magmatism-dominated intracontinental rifting in the Mesoproterozoic: The Ngaanyatjarra Rift, central Australia, Gondwana Research, 24(3–4), 886–901, doi:10.1016/j.gr.2012.10.003, 2013.

Altenberger, U., Prosser, G., Ruggiero, M. and Gunter, C.: Microstructure and petrology of a Calabrian garnet-bearing pseudotachylyte - a link to lower-crustal seismicity, Geological Society, London, Special Publications, 359(1), 153–168, doi:10.1144/SP359.9, 2011.

Altenberger, U., Prosser, G., Grande, A., Günter, C. and Langone, A.: A seismogenic zone in the deep crust indicated by pseudotachylytes and ultramylonites in granulite-facies rocks of Calabria (Southern Italy), Contributions to Mineralogy and Petrology, 166(4), 975–994, doi:10.1007/s00410-013-0904-3, 2013.

Austrheim, H.: Fluid and deformation induced metamorphic processes around Moho beneath continent collision zones: Examples from the exposed root zone of the Caledonian mountain belt, W-Norway, Tectonophysics, 609, 620–635, doi:10.1016/j.tecto.2013.08.030, 2013.

Austrheim, H. and Boundy, T. M.: Pseudotachylytes Generated During Seismic Faulting and Eclogitization of the Deep Crust, Science, 265(5168), 82–83, doi:10.1126/science.265.5168.82, 1994.

Austrheim, H., Erambert, M. and Boundy, T. M.: Garnets recording deep crustal earthquakes, Earth and Planetary Science Letters, 139(1–2), 223–238, doi:10.1016/0012-821X(95)00232-2, 1996.

23

Deleted: Wisconson

Deleted: .
—————————Page Break—————————

620 Austrheim, H., Dunkel, K. G., Plümper, O., Ildefonse, B., Liu, Y. and Jamtveit, B.: Fragmentation of wall rock garnets
621 during deep crustal earthquakes, Science Advances, 3(2), e1602067, doi:10.1126/sciadv.1602067, 2017.

622 Burov, E. B. and Watts, A. B.: The long-term strength of continental lithosphere: "jelly sandwich" or "crème brûlée"?,
623 GSA Today, 16(1), 4, doi:10.1130/1052-5173(2006)016<4:TLTSOC>2.0.CO;2, 2006.

624 Camacho, A. and Fanning, C. M.: Some isotopic constraints on the evolution of the granulite and upper amphibolite
625 facies terranes in the eastern Musgrave Block, central Australia, Precambrian Research, 71(1), 155–181, 1995.

626 Camacho, A. and McDougall, I.: Intracratonic, strike-slip partitioned transpression and the formation and exhumation
627 of eclogite facies rocks: An example from the Musgrave Block, central Australia, Tectonics, 19(5), 978–996, 2000.

628 Camacho, A., Vernon, R. H. and Fitz Gerald, J. D.: Large volumes of anhydrous pseudotachylyte in the Woodroffe
629 Thrust, eastern Musgrave Ranges, Australia, Journal of Structural Geology, 17(3), 371–383, 1995.

630 Camacho, A., Compston, W., McCulloch, M. and McDougall, I.: Timing and exhumation of eclogite facies shear
631 zones, Musgrave Block, central Australia, J. metamorphic Geol., 15, 735–751, 1997.

632 Clarke, G. L. and Norman, A. R.: Generation of pseudotachylite under granulite facies conditions, and its preservation
633 during cooling, Journal of Metamorphic Geology, 11(3), 319–335, doi:10.1111/j.1525-1314.1993.tb00151.x, 1993.

634 Connolly, J. A. D.: Multivariable phase diagrams; an algorithm based on generalized thermodynamics, American
635 Journal of Science, 290(6), 666–718, doi:10.2475/ajs.290.6.666, 1990.

636 Deichmann, N. and Rybach, L.: Earthquakes and temperatures in the lower crust below the northern Alpine foreland
637 of Switzerland, Properties and processes of earth's lower crust, 197–213, 1989.

638 Di Toro, G. and Pennacchioni, G.: Superheated friction-induced melts in zoned pseudotachylytes within the Adamello
639 tonalites (Italian Southern Alps), Journal of Structural Geology, 26(10), 1783–1801, doi:10.1016/j.jsg.2004.03.001,
640 2004.

641 Duputel, Z., Vergne, J., Rivera, L., Wittlinger, G., Farra, V. and Hetényi, G.: The 2015 Gorkha earthquake: A large
642 event illuminating the Main Himalayan Thrust fault, Geophysical Research Letters, 43(6), 2517–2525,
643 doi:10.1002/2016GL068083, 2016.

644 Ellis, D. J. and Maboko, M. A. H.: Precambrian tectonics and the physicochemical evolution of the continental crust.
645 I. The gabbro-eclogite transition revisited, Precambrian Research, 55(1), 491–506, 1992.

646 Ellis, S. and Stöckhert, B.: Elevated stresses and creep rates beneath the brittle-ductile transition caused by seismic
647 faulting in the upper crust, Journal of Geophysical Research, 109(B5), doi:10.1029/2003JB002744, 2004.

648 Evins, P. M., Smithies, R. H., Howard, H. M., Kirkland, C. L., Wingate, M. T. D. and Bodorkos, S.: Redefining the
649 Giles Event within the setting of the 1120-1020 Ma Ngaanyatjarra Rift, West Musgrave Province, Central Australia,
650 Geological Society of Western Australia, East Perth, W.A., 2010.

651 Fitz Gerald, J. D., Mancktelow, N. S., Pennacchioni, G. and Kunze, K.: Ultrafine-grained quartz mylonites from high-
652 grade shear zones: Evidence for strong dry middle to lower crust, Geology, 34(5), 369, doi:10.1130/G22099.1, 2006.

653 Förster, H.-J. and Harlov, D. E.: Monazite-(Ce)–huttonite solid solutions in granulite-facies metabasites from the
654 Ivrea-Verbano Zone, Italy, Mineralogical Magazine, 63(4), 587–587, 1999.

655 Glikson, A. Y. and Australian Geological Survey Organisation, Eds.: Geology of the western Musgrave Block, central
656 Australia, with particular reference to the mafic-ultramafic Giles Complex, Australian Govt. Pub. Service, Canberra,
657 1996.

658 Goetze, C. and Evans, B.: Stress and temperature in the bending lithosphere as constrained by experimental rock
659 mechanics, Geophysical Journal International, 59(3), 463–478, 1979.

660 Gray, C. M.: Geochronology of granulite-facies gneisses in the western Musgrave Block, Central Australia, Journal
661 of the Geological Society of Australia, 25(7–8), 403–414, doi:10.1080/00167617808729050, 1978.

662 Handy, M. and Brun, J.-P.: Seismicity, structure and strength of the continental lithosphere, Earth and Planetary
663 Science Letters, 223(3–4), 427–441, doi:10.1016/j.epsl.2004.04.021, 2004.

664 Hobbs, B. E., Ord, A. and Teyssier, C.: Earthquakes in the Ductile Regime?, PAGEOPH, 124(1), 309–336, 1986.

665 Holland, T. J. B. and Powell, R.: An internally consistent thermodynamic data set for phases of petrological interest,
666 Journal of metamorphic Geology, 16(3), 309–343, 1998.

667 Jackson, J.: Faulting, flow, and the strength of the continental lithosphere, International Geology Review, 44(1), 39–
668 61, 2002a.

669 Jackson, J.: Strength of the continental lithosphere: Time to abandon the jelly sandwich?, GSA Today, 12(9), 4,
670 doi:10.1130/1052-5173(2002)012<0004:SOTCLT>2.0.CO;2, 2002b.

671 Jackson, J. A., Austrheim, H., McKenzie, D. and Priestley, K.: Metastability, mechanical strength, and the support of
672 mountain belts, Geology, 32(7), 625–628, 2004.

673 John, T., Medvedev, S., Rüpke, L. H., Andersen, T. B., Podladchikov, Y. Y. and Austrheim, H.: Generation of
674 intermediate-depth earthquakes by self-localizing thermal runaway, Nature Geoscience, 2(2), 137–140,
675 doi:10.1038/ngeo419, 2009.

676 Kirkpatrick, J. D. and Rowe, C. D.: Disappearing ink: How pseudotachylytes are lost from the rock record, Journal of
677 Structural Geology, 52, 183–198, doi:10.1016/j.jsg.2013.03.003, 2013.

678 Kohlstedt, D. L., Evans, B. and Mackwell, S. J.: Strength of the lithosphere: Constraints imposed by laboratory
679 experiments, Journal of Geophysical Research: Solid Earth, 100(B9), 17587–17602, doi:10.1029/95JB01460, 1995.

680 Lambert, I. B. and Heier, K. S.: Geochemical investigations of deep-seated rocks in the Australian shield, Lithos, 1(1),
681 30–53, doi:10.1016/S0024-4937(68)80033-7, 1968.

682 Lanari, P., Vidal, O., De Andrade, V., Dubacq, B., Lewin, E., Grosch, E. G. and Schwartz, S.: XMapTools: A
683 MATLAB©-based program for electron microprobe X-ray image processing and geothermobarometry, Computers &
684 Geosciences, 62, 227–240, doi:10.1016/j.cageo.2013.08.010, 2014.

685 Li, Z.-X. and Evans, D. A.: Late Neoproterozoic 40 intraplate rotation within Australia allows for a tighter-fitting and
686 longer-lasting Rodinia, Geology, 39(1), 39–42, 2011.

687 Lin, A., Maruyama, T., Aaron, S., Michibayashi, K., Camacho, A. and Kano, K.: Propagation of seismic slip from
688 brittle to ductile crust: Evidence from pseudotachylyte of the Woodroffe thrust, central Australia, Tectonophysics,
689 402(1–4), 21–35, doi:10.1016/j.tecto.2004.10.016, 2005.

690 Lund, M. G. and Austrheim, H.: High-pressure metamorphism and deep-crustal seismicity: evidence from
691 contemporaneous formation of pseudotachylytes and eclogite facies coronas, Tectonophysics, 372(1–2), 59–83,
692 doi:10.1016/S0040-1951(03)00232-4, 2003.

693 Maddock, R. H., Grocott, J. and Van Nes, M.: Vesicles, amygdales and similar structures in fault-generated
694 pseudotachylytes, Lithos, 20(5), 419–432, 1987.

25

695 Major, R. B. and Conor, C. H. H.: The Musgrave Block. In: J.F. Drexel, W.P. Preiss and A.J. Parker (Editors), The
696 Geology of South Australia, Vol.1. The Precambrian, Geological Survey of South Australia, Bulletin 54, pp. 156-167,
697 1993.

698 McKenzie, D. and Brune, J. N.: Melting on fault planes during large earthquakes, Geophysical Journal International,
699 29(1), 65–78, 1972.

700 Menegon, L., Nasipuri, P., Stünitz, H., Behrens, H. and Ravna, E.: Dry and strong quartz during deformation of the
701 lower crust in the presence of melt, Journal of Geophysical Research, 116(B10), doi:10.1029/2011JB008371, 2011.

702 Menegon, L., Pennacchioni, G., Malaspina, N., Harris, K. and Wood, E.: Earthquakes as Precursors of Ductile Shear
703 Zones in the Dry and Strong Lower Crust, Geochemistry, Geophysics, Geosystems, 18(12), 4356–4374,
704 doi:10.1002/2017GC007189, 2017.

705 Mitra, S., Priestley, K., Bhattacharyya, A. K. and Gaur, V. K.: Crustal structure and earthquake focal depths beneath
706 northeastern India and southern Tibet: Crustal structure beneath NE India, Geophysical Journal International, 160(1),
707 227–248, doi:10.1111/j.1365-246X.2004.02470.x, 2004.

708 Moecher, D. P. and Steltenpohl, M. G.: Direct calculation of rupture depth for an exhumed paleoseismogenic fault
709 from mylonitic pseudotachylyte, Geology, 37(11), 999–1002, 2009.

710 Moecher, D. P. and Steltenpohl, M. G.: Petrological evidence for co-seismic slip in extending middle-lower
711 continental crust: Heier's zone of pseudotachylyte, north Norway, Geological Society, London, Special Publications,
712 359(1), 169–186, doi:10.1144/SP359.10, 2011.

713 Milligan, P. R. and Nakamura, A.: Total Magnetic Intensity (TMI) image 2015 greyscale, Geoscience Australia
714 doi:10.4225/25/574CF5E15C119, 2015.

715 Edgoose, C. J., Close, D. F. and Scrimgeour, I.: Australia 1:250 000 geological series, Sheet SG 52-7, Northern
716 Territory Department of Mines and Energy, 1999.

717 Orlandini, O., Mahan, K. H., Regan, S., Williams, M. L. and Leite, A.: Pseudotachylytes of the Deep Crust: Examples
718 from a Granulite-Facies Shear Zone, AGU Fall Meeting Abstracts, T53C–2606, 2013.

719 Pennacchioni, G. and Cesare, B.: Ductile-brittle transition in pre-Alpine amphibolite facies mylonites during evolution
720 from water-present to water-deficient conditions (Mont Mary nappe, Italian Western Alps), Journal of Metamorphic
721 Geology, 15(6), 777–791, 1997.

722 Pittarello, L., Pennacchioni, G. and Di Toro, G.: Amphibolite-facies pseudotachylytes in Premosello metagabbro and
723 felsic mylonites (Ivrea Zone, Italy), Tectonophysics, 580, 43–57, doi:10.1016/j.tecto.2012.08.001, 2012.

724 Price, N. A., Johnson, S. E., Gerbi, C. C. and West, D. P.: Identifying deformed pseudotachylyte and its influence on
725 the strength and evolution of a crustal shear zone at the base of the seismogenic zone, Tectonophysics, 518–521, 63–
726 83, doi:10.1016/j.tecto.2011.11.011, 2012.

727 Rao, N. P., Tsukuda, T., Kosuga, M., Bhatia, S. C. and Suresh, G.: Deep lower crustal earthquakes in central India:
728 inferences from analysis of regional broadband data of the 1997 May 21, Jabalpur earthquake, Geophysical Journal
729 International, 148(1), 132–138, 2002.

730 Reyners, M., Eberhart-Phillips, D. and Stuart, G.: The role of fluids in lower-crustal earthquakes near continental rifts,
731 Nature, 446(7139), 1075–1078, doi:10.1038/nature05743, 2007.

732 Geological Survey of South Australia: Dataset SA_RAD_TH, Thorium map of South Australia, 2011

733 Scharbert, P. D. H. G., Korkisch, P. D. J. and Steffan, D. I.: Uranium, thorium and potassium in granulite facies rocks,
734 Bohemian Massif, Lower Austria, Austria, Tschermaks Petr. Mitt., 23(4), 223–232, doi:10.1007/BF01083102, 1976.

26

735 Sclater, J. G., Jaupart, C. and Galson, D.: The heat flow through oceanic and continental crust and the heat loss of the
736 Earth, Reviews of Geophysics, 18(1), 269, doi:10.1029/RG018i001p00269, 1980.

737 Scrimgeour, I. R. and Close, D. F.: Regional high-pressure metamorphism during intracratonic deformation: the
738 Petermann Orogeny, central Australia, Journal of Metamorphic Geology, 17, 557–572, 1999.

739 Sibson, R. H.: Generation of pseudotachylyte by ancient seismic faulting, Geophysical Journal International, 43(3),
740 775–794, 1975.

741 Sibson, R. H.: Transient discontinuities in ductile shear zones, Journal of Structural Geology, 2(1), 165–171, 1980.

742 Sibson, R. H. and Toy, V. G.: The habitat of fault-generated pseudotachylyte: Presence vs. absence of friction-melt,
743 in Geophysical Monograph Series, vol. 170, edited by R. Abercrombie, A. McGarr, H. Kanamori, and G. Di Toro, pp.
744 153–166, American Geophysical Union, Washington, D. C., 2006.

745 Singer, J., Diehl, T., Husen, S., Kissling, E. and Duretz, T.: Alpine lithosphere slab rollback causing lower crustal
746 seismicity in northern foreland, Earth and Planetary Science Letters, 397, 42–56, doi:10.1016/j.epsl.2014.04.002,
747 2014.

748 Smithies, R. H., Howard, H. M., Evins, P. M., Kirkland, C. L., Kelsey, D. E., Hand, M., Wingate, M. T. D., Collins,
749 A. S. and Belousova, E.: High-Temperature Granite Magmatism, Crust-Mantle Interaction and the Mesoproterozoic
750 Intracontinental Evolution of the Musgrave Province, Central Australia, Journal of Petrology, 52(5), 931–958,
751 doi:10.1093/petrology/egr010, 2011.

752 Steltenpohl, M. G., Kassos, G. and Andresen, A.: Retrograded eclogite-facies pseudotachylytes as deep-crustal
753 paleoseismic faults within continental basement of Lofoten, north Norway, Geosphere, 2(1), 61–72,
754 doi:10.1130/GES00035.1, 2006.

755 Thielmann, M., Rozel, A., Kaus, B. J. P. and Ricard, Y.: Intermediate-depth earthquake generation and shear zone
756 formation caused by grain size reduction and shear heating, Geology, 43(9), 791–794, doi:10.1130/G36864.1, 2015.

757 Trepmann, C. A. and Stöckhert, B.: Cataclastic deformation of garnet: a record of synseismic loading and postseismic
758 creep, Journal of Structural Geology, 24(11), 1845–1856, doi:10.1016/S0191-8141(02)00004-4, 2002.

759 Ueda, T., Obata, M., Di Toro, G., Kanagawa, K. and Ozawa, K.: Mantle earthquakes frozen in mylonitized ultramafic
760 pseudotachylytes of spinel-lherzolite facies, Geology, 36(8), 607, doi:10.1130/G24739A.1, 2008.

761 Wade, B. P., Barovich, K. M., Hand, M., Scrimgeour, I. R. and Close, D. F.: Evidence for early Mesoproterozoic arc
762 magmatism in the Musgrave Block, central Australia: implications for Proterozoic crustal growth and tectonic
763 reconstructions of Australia, The Journal of geology, 114(1), 43–63, 2006.

764 Wenk, H. R. and Weiss, L. E.: Al-rich calcic pyroxene in pseudotachylyte: An indicator of high pressure and high
765 temperature?, Tectonophysics, 84, 329–341, 1982.

766 Wex, S., Mancktelow, N. S., Hawemann, F., Camacho, A. and Pennacchioni, G.: Geometry of a large-scale, low-
767 angle, mid-crustal thrust (Woodroffe Thrust, central Australia), Tectonics, doi:10.1002/2017TC004681, 2017.

768 White, J. C.: Transient discontinuities revisited: pseudotachylyte, plastic instability and the influence of low pore fluid
769 pressure on deformation processes in the mid-crust, Journal of Structural Geology, 18(12), 1471–1486, 1996.

770 White, J. C.: Instability and localization of deformation in lower crust granulites, Minas fault zone, Nova Scotia,
771 Canada, Geological Society, London, Special Publications, 224(1), 25–37, doi:10.1144/GSL.SP.2004.224.01.03,
772 2004.

27

773 White, J. C.: Paradoxical pseudotachylyte – Fault melt outside the seismogenic zone, Journal of Structural Geology,
774 38, 11–20, doi:10.1016/j.jsg.2011.11.016, 2012.

775 Xu, Y., Roecker, S. W., WEI, R.-P., ZHANG, W.-L. and WEI, B.: Analysis of Seismic Activity in the Crust from
776 Earthquake Relocation in the Central Tien Shan, Chinese Journal of Geophysics, 48(6), 1388–1396, 2005.

777 Zhao, J., McCulloch, M. and Korsch, R. J.: Characterisation of a plume-related ~ 800 Ma magmatic event and its
778 implications for basin formation in central-southern Australia, Earth and Planetary Science Letters, 121, 349–367,
779 1994.